

## ABSTRACT

Title of Thesis:       **PIEZOELECTRIC SENSING AND ENERGY  
HARVESTING IN TOUCHSCREENS**

Team Piezo: Jacob Bremerman, Bachelor of Science Physics, Bachelor of Arts Spanish, 2017, Steven Bronocco, Bachelor of Arts Economics, Bachelor of Arts Criminology and Criminal Justice, 2017, Brenden Caffey, Bachelor of Science Electrical Engineering, 2017, Terri Kent, Bachelor of Science Mechanical Engineering, 2017, Eric Lee, Bachelor of Science Chemical Engineering, 2017, Rounak Mukhopadhyay, Bachelor of Science Aerospace Engineering, 2017, Anand Patel, Bachelor of Science Aerospace Engineering, Emily Reed, Bachelor of Science Chemistry, 2017, Chris Rother, Bachelor of Science Mechanical Engineering, 2017, Adam Stambouli, Bachelor of Science Aerospace Engineering, 2017, Erin Verni, Bachelor of Science Mechanical Engineering, 2017, Torrance Wang, Bachelor of Science Bioengineering, 2017

Thesis directed by:   Dr. Bao Yang, Department of Mechanical Engineering

Team Piezo investigated the increasing demands on smartphone batteries by developing a touchscreen prototype that integrates piezoelectric materials to sense touch location and generate energy for the battery. The touchscreen prototype uses a piezoelectric element with patterned electrodes that extract a current when touched. A circuit with an Arduino microcontroller successfully senses the location of the activated piezoelectric sections. The team designed several prototypes and conducted testing to evaluate performance and electrical response. Methods of extracting and storing energy were investigated, however storage was not successful enough to integrate into the prototype. Phone usage data was collected with surveys and was compared to power output of the touchscreen system to determine the theoretical amount of retrievable energy for future development.

PIEZOELECTRIC SENSING AND ENERGY HARVESTING IN  
TOUCHSCREENS

by

Team Piezo:

Jacob Bremerman, Steven Bronocco, Brenden Caffey, Terri Kent, Emily Reed, Eric  
Lee, Rounak Mukhopadhyay, Anand Patel, Emily Reed, Chris Rother, Adam  
Stambouli, Erin Verni, Torrance Wang,

Thesis submitted in partial fulfillment of the requirements of the  
Gemstone Program, University of Maryland,  
2017

Advisory Committee:

Dr. Bao Yang, Chair

Mr. Jim Miller, Team Librarian

Ms. Marybeth Shea

Dr. Aris Christou

Dr. Yunho Hwang

Dr. Wei Luo

© Copyright by  
Jacob Bremerman, Steven Bronocco, Brenden Caffey, Terri Kent, Emily Reed, Eric  
Lee, Rounak Mukhopadhyay, Anand Patel, Emily Reed, Chris Rother, Adam  
Stambouli, Erin Verni, Torrance Wang,  
2017

## Acknowledgements

Team Piezo would like to acknowledge the Gemstone staff: Dr. Coale, Dr. Skendall, Leah Kreimer Tobin, and Vickie Hill for all their support throughout this process. We would also like to thank our mentor, Dr. Bao Yang, for his guidance and assistance with our research. We would like to recognize our librarians, Alex Carroll and Jim Miller for their help with our literature review and patent search. We also could not have completed our prototype fabrication without the help of Thomas Loughran and the Maryland NanoCenter FabLab staff. In addition, Andrea Dragan and the Institutional Review Board staff were essential to the success of our surveys. Finally, the team would like to acknowledge the University of Maryland Sustainability Fund and the Office of Technology and Commercialization for their support. Thank you!

# Table of Contents

Acknowledgements.....	iv
Table of Contents.....	v
Chapter 1: Introduction.....	1
Chapter 2: Literature Review.....	2
2.1 Background of Piezoelectrics and Current Applications.....	2
2.2 Application of Piezoelectrics to Electronic Devices.....	3
2.2.1 Power Generation and Storage.....	3
2.2.2 Current Touchscreen Technology.....	4
2.2.3 Types of Piezoelectric Materials and Configurations.....	5
Chapter 3: Methodology.....	7
3.1. Surveys.....	7
3.1.1 Usage Survey.....	7
3.1.2 Pressure Survey.....	7
3.2 General Experimentation/Preliminary Testing.....	8
3.2.1 Piezoelectric Material Selection.....	8
3.2.2 Touchscreen System Modeling.....	9
3.2.3 Force vs. Voltage.....	12
3.3 Circuit Design for Power Storage.....	15
3.4 Prototype.....	17
3.4.1 Grid Design.....	17
3.4.2 Voltage, Power, Waveform Characteristics.....	22
3.4.3 Arduino Prototype.....	23
Chapter 4: Results and Discussion.....	27
4.1 Surveys.....	27
4.2 General Experimentation/Preliminary Testing.....	29
4.2.1 Piezoelectric Material Selection.....	29
4.2.2 Touchscreen System Modeling.....	29
4.2.3 Force vs. Voltage.....	40
4.3 Circuits and Power Generation.....	42
4.4 Prototyping.....	46
4.4.1 Voltage, Power, Waveform Characteristics.....	46
4.4.2 Arduino Prototype.....	54
Chapter 5: Conclusion.....	56
5.1 Summary of Results.....	56
5.2 Contributions.....	56
5.3 Recommendations for Future Work.....	57
Glossary.....	59
Bibliography.....	62

## Chapter 1: Introduction

Since the introduction of the iPhone in 2007, an increasing number of people have access to smartphone technology with 1.64 billion consumers worldwide as of 2014 (eMarketer, 2014). Because of increase in functionality, smartphones that deplete their batteries in a single day are replacing old cell phones with batteries that last for a week between charges. The energy used to power one phone is 1kWh per year (Helman, 2013). Thus, the energy to power all the phones currently in use in the world is about 1.64 billion kWh per year, which translates to about one billion kg of CO<sub>2</sub> emissions per year from coal sources (EPA, 2014). Although smartphones are only one source of pollution, reducing their carbon footprint will decrease total emission levels. Piezoelectric materials can be applied to smartphones to make their energy use cleaner.

Piezoelectric materials are those with the ability to convert mechanical energy to electrical energy and vice versa. Many current applications are large scale, such as the floor tiles in Japan's Tokyo subway station that use pressure from footsteps to power nearby lights (Ryall, 2008; Henderson, 2009). This technology is not applied as extensively on a smaller scale. In a smartphone application, the taps on the phone touchscreen will act similar to a person's footsteps on the piezoelectric floor tiles in the larger scale application to generate energy.

Team Piezo chose to focus on piezoelectric energy harvesting based on a common interest in underutilized sources of renewable energy. Smartphone touchscreens were chosen as the application because forces are frequently applied during normal use. Team Piezo's work supplemented current research by developing a functional piezoelectric touchscreen with the potential to generate useful energy. The goal of the project was to create a proof of concept prototype that showcases the developed technology without necessarily matching current smartphone dimensions and functionality. Team Piezo aimed to answer the following research question: how can piezoelectric materials be used in a touchscreen to accurately detect the location of applied pressure and to harvest energy in order to extend smartphone battery life?

## Chapter 2: Literature Review

### 2.1 Background of Piezoelectrics and Current Applications

Piezoelectric materials belong to a broader class called ferroelectrics. One of the defining traits of a ferroelectric material is that the molecular structure is oriented such that the material has local charge separations, known as electric dipoles (Sodano, 2004). Piezoelectric materials have two main functions. The first function is the direct piezoelectric effect, which is the transformation of mechanical strain into electrical charge. The second function, called the converse piezoelectric effect, takes an applied electrical potential and converts to mechanical strain (Sodano, 2004). Therefore, an electric field can be applied to induce an expansion or contraction of the material and vice versa.

The piezoelectric effect occurs due to the material's electric dipoles (Telba, 2012). Dipoles are represented as vectors pointing from the positive to the negative charges. Groups of aligned dipoles are called Weiss domains. In a piezoceramic material, which are materials that are not inherently piezoelectric like naturally-occurring piezoelectric crystals, but rather can be manipulated to exhibit piezoelectric behavior, the Weiss domains are not aligned, and the overall material has no net polarization. After applying an electric field, the domains align themselves in the direction of the field, creating a polarization.

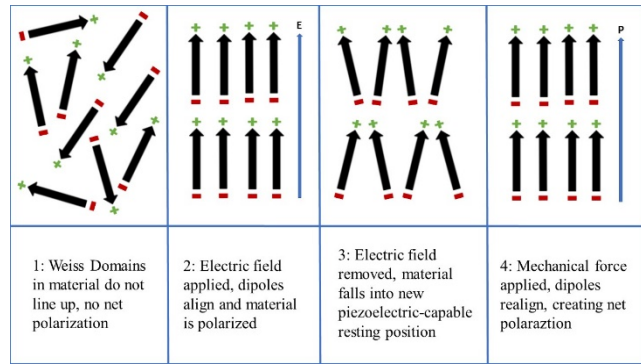


Figure 1: Weiss domains before during and after polarization. Balance of charges is disrupted to create a potential difference

When the field is removed, the material cannot return to its original structure, but rather a more organized structure which allows for the material to exhibit the piezoelectric effects like a normal crystal. Applying mechanical stress to this newly piezoelectric material disrupts the orientation of the dipoles, realigning them as they were during polarization with the applied electric field and bringing about a polarization which creates a potential difference across the material. This voltage drop allows charge to flow between the two poles in order to realign the dipoles, thus generating a current. Additionally, the applied pressure and the generated energy have a direct relationship in which increasing the pressure will also increase the energy output (Woodford, 2014).

The piezoelectric charge coefficient,  $d_{xx}$ , gives the amount of electrical charge to the strain applied in units of picocoulombs ( $10^{-12}$  coulombs) per Newton in one of the six directions. The  $d_{33}$  value gives the charge on the top and bottom of the piezoelectric when a force is applied to the top of the piezoelectric. Natural piezoelectric crystals, such as quartz, typically have lower piezoelectric charge coefficients than synthetic piezoelectric materials (Prasannablalaji, 2013). Team Piezo's touchscreen prototype uses one of the most common and efficient synthetic

piezoelectric materials, lead-zirconate-titanate (PZT) ceramic (Goldfarb, 1999). A frequent application of this material is a PZT stack, which is made by mechanically assembling several PZT wafers in series and then connecting the electrodes so that the wafers are in parallel electrically as seen in Figure 2.

The wafers are polarized in the same direction along their thickness. This uniaxial polarization means that the stack exhibits the piezoelectric effect only in the vertical direction (Goldfarb, 1999). When a voltage is applied across the electrodes, the stack elongates in this vertical direction. Conversely, when the stack is vertically compressed or elongated, an electric current is generated.

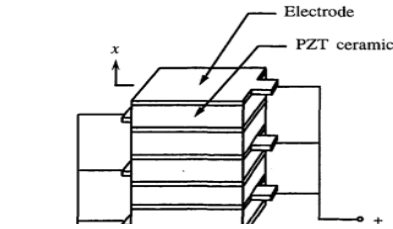


Figure 2: Illustration of a PZT stack (Goldfarb, 1999)

## 2.2 Application of Piezoelectrics to Electronic Devices

### 2.2.1 Power Generation and Storage

When considering the possibilities for energy generation from a piezoelectric device, energy storage is a major hurdle. Once mechanical energy is converted to electrical energy, it can either be used directly or stored in a battery. For any normal touchscreen device to operate, it needs a constant direct current (DC) power source. This is true of modern computers, smartphones, and any other electronic device that uses a battery. For the purposes of a non-resonant piezoelectric power generation device, the energy must be stored. A piezoelectric touchscreen is non-resonant because it experiences irregular excitation and does not generate a steady signal; therefore, it is not a suitable direct power source. Therefore, any attempts to produce and use energy from this touchscreen must be stored in a battery that is representative of batteries in modern touchscreen devices.

Team Piezo’s focus, modern smartphones, use lithium-ion batteries because the performance does not decay as much as nickel-cadmium (NiCd) and nickel-metal-hydride (NiMH) battery alternatives (Charging lithium ion batteries, 2003). Unlike lithium-ion batteries, the lesser alternatives must be fully discharged and recharged when used to prevent battery life reduction. Although the output is generally low, piezoelectric devices are capable of charging lithium ion batteries through mechanical vibrations at resonant frequencies and harmonics (Huq & Williamson 2013). It may be possible to make use of similar circuitry to charge a battery with non-resonant mechanical deformations.

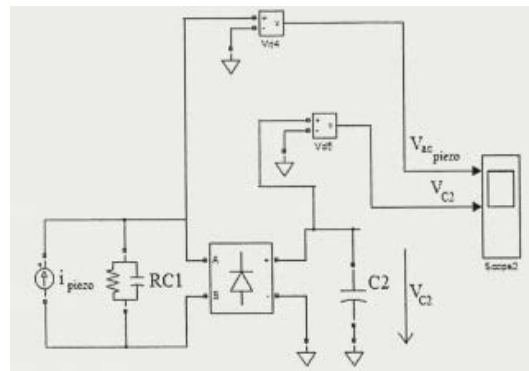


Figure 3: AC/DC converter circuit diagram



Researchers have experimented with applications of piezoelectricity as an alternative source of energy for batteries similar to those of smartphones. In one study from the University of Oradea in Romania, a variety of piezoelectric crystals were used with an AC/DC power converter so that the machine would convert the generated alternating current (AC) into direct current (DC) to power an electronic device (Neamtu & Kokkosis, 2012). The researchers used a lithium-ion battery with polyvinylidene fluoride (PVDF), PZT, and MFC crystals. The researchers measured the battery's state of charge (SOC), which is a rating from 0 to 100 percent of how charged the battery is. The battery's average SOC with the three types of crystals increased by 0.001% over a span of seven seconds, 2.8% in an hour, and 67% in the total 24-hour time frame. Additionally, researchers from the University of Malaysia in Sabah conducted trials with a 12-V NiMH battery and pieces of piezoelectric film (Dayou, Man-Sang *et al*, 2009). A single piezoelectric film strip produced a root mean square voltage of 1.18 V to the 12-V battery and a later discharge of 0.9 W over the span of an hour. This discharge showed that a piezoelectric film wattage can be used to enhance the smartphone battery power by a small amount. Both research articles show that piezoelectrics produce small amounts of power but that these small wattages can increase the charge of a smartphone battery. Research indicates there are several existing avenues that may be viable for charging a battery with a piezoelectric touchscreen which were investigated within Team Piezo's testing process.

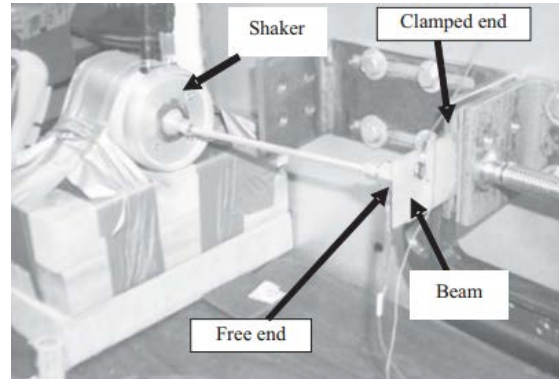


Figure 4: Experimental setup for piezoelectric battery charging (Dayou, Man-Sang *et al*, 2009).

### 2.2.2 Current Touchscreen Technology

In order to develop a touchscreen with piezoelectric materials, current touchscreen technology must be evaluated. Within the past decade, the number of touchscreen applications has significantly increased (Touching the future, 2008). The three types of modern touchscreens are resistive, infrared, and capacitive.

Resistive touchscreens are found in many devices including the Nintendo DS and phones such as the Samsung Instinct (How does a touchscreen phone work?, 2011). These touchscreens use a multi-layered design that requires an applied pressure to physically deform the screen. Below layers of circuit-transmitting material, small bumps separate the currents. When

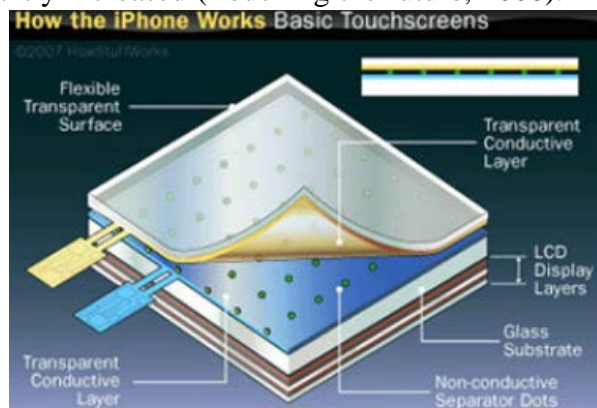


Figure 5: Construction of a resistive touchscreen (Wilson, Chandler, Fenlon, & Johnson, 2007).

pressure is applied, the top layer is pushed into the lower layer, thus disturbing the current. The phone then uses this disturbance to locate where the force was applied on the touchscreen. (PhoneArena Team, 2008). Benefits of resistive touchscreens are its low cost and the ability of the screen to recognize any material. However, drawbacks include the screen's increased susceptibility to scratches, lack of multi-touch capabilities, and limited visibility in the sun.

Infrared touchscreens are the least common type and are found only in a few devices such as the Samsung U600 and the Neonode N2 (How does a touchscreen phone work?, 2011). These touchscreens are based on thermal or optical processes. For thermal screens, the heat from a finger is detected and used to determine the location. In optical screens, lasers are fired above the screen that detect the location of a material based on where the lasers are interrupted (Teiche *et al.*, 2009). This technology is the most expensive of the three, and for thermal screens, only a bare finger or compatible heat source can be used. However, laser screens can sense contact from any material, like for resistive touchscreens.

Finally, capacitive touchscreens are found in common smartphone devices such as the iPhone and the Samsung Galaxy (How does a touchscreen phone work?, 2011). These screens sense location using the electrons from your finger rather than deformation caused by an applied force. In capacitive screens, a voltage is applied to a conductive layer formed by a grid of wires, creating an electric field. When electrons from a finger come into close proximity with the screen, the circuit is grounded through the finger, which creates a voltage drop. A microcontroller detects the voltage drop and uses it to determine the touch location (Saini, 2011). This technology has good visibility in the sun and multi-touch capabilities. However, capacitive touchscreens are more expensive than resistive touchscreens, and a finger, or specially made stylus, must be used.

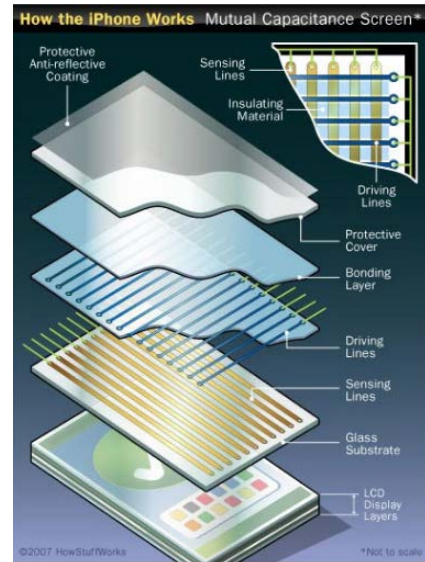


Figure 6: Construction of a capacitive touchscreen (Wilson, Chandler, Fenlon, & Johnson, 2007).

Team Piezo's design most closely resembles that of a resistive touchscreen because it relies on deformation. A flexible top layer allows deformation of the piezoelectric film, which tracks the contact point by detecting current from the specific piezoelectric grid element where pressure was applied.

### 2.2.3 Types of Piezoelectric Materials and Configurations

The piezoelectric coefficient ( $d_{33}$  value) of several widely used piezoelectric materials, which are representative of their power outputs, are listed in Table 1. Piezoelectrics are generally evaluated by their  $d_{33}$  values because the values show the coulombs generated over the force in the perpendicular direction (Sirohi & Inderjit, 2000). PZT, KNN-LT-LS, and PZN-9PT have high  $d_{33}$  values and could be suitable for energy harvesting applications.

However, PZT and PZN-9PT are lead-based. The environmental and human health concerns of using lead could dissuade the target interest group.

Using KNN-LT-LS or other non-lead materials would be preferable for use in a smartphone even though lead-based compounds tend to have higher  $d_{33}$  values. KNN-LT-LS is listed because it is one of the few non-lead-based compounds that has comparable  $d_{33}$  values to the lead-based compounds (Choy, 2007; Zhao et al., 2007).

The majority of research in the field of piezoelectric power harvesting is based on wind or other sources of energy that can generate resonant excitation, which is characterized by regular motion with similar frequencies. In contrast, a touchscreen receives impulses of varying intensities over irregular time intervals. If a significant amount of energy is to be gathered, the system must be optimized for this source. The method of mounting the piezoelectric tile also affects the system's performance by dictating the displacement due to an applied force. One research team addressed non-resonant systems by designing a bi-stable mounting system, as shown in Figure 7. A small force could create a large amount of motion by pushing the mount out of its first stable state and causing it to fall into a second stable state. Another force would be able to reverse the process.

Researchers have also improved the performance of energy harvesting piezoelectric systems by patterning the electrodes and modifying the polarization of the material. In a study from the University of Pittsburgh, researchers found that reversing the polarization of the outer section of a circular piezoelectric wafer to match the reversed stress improved the energy generation. The electrodes of the wafer also had to be patterned to avoid destructive interference by creating electrical separation between the inner and outer sections. The researchers used an acid-resistant ink mask to define the pattern and ferric chloride acid ( $\text{FeCl}_3$ ) as an etchant to remove part of the electrodes (Kim, 2005). Team Piezo's design uses this concept of electrical separation in the electrode layers of a piezoelectric tile to create a touchscreen capable of location sensing.

Table 1: Various man-made piezoelectric materials with their respective  $d_{33}$  values (Prasannablalaji, 2014; Piezotech, n.d.; Abazari, 2008; Pavlic, 2014).

Piezoelectric material	$d_{33}$ ( $10^{-12}\text{C/N}$ )
PZT	560
PVDF	13-22
KNN	80-120
Quartz	2.3
PZN-9PT	2500
$\text{PbTiO}_3$	120
$\text{BaTiO}_3$	90
KNN-LT-LS	416

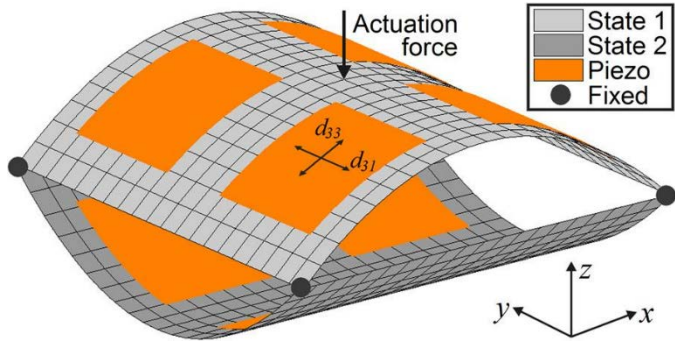


Figure 7: A bi-stable mounting system. (Betts, Kim, Bowen, & Inman, 2012)

## Chapter 3: Methodology

Team Piezo focused on the following research question: how can piezoelectric sensors be utilized in a touchscreen to detect the location of applied pressure on the screen and to harvest energy in order to extend smartphone battery life? The team showed that a piezoelectric grid can be used as a sensor to show where pressure is applied. Additionally, the team hoped to show that a touchscreen with an added piezoelectric layer is able to generate enough electricity from a user tapping the phone to make the new screen comparable to alternative power sources for smartphones. The team conducted surveys and collected data in order to determine the average pressure a user applies to a phone. This pressure was used in conjunction with the team's lab research to determine how much energy the piezoelectric layer can generate. Team Piezo's research provided necessary knowledge for creating a smartphone with a piezoelectric screen that generates electricity to supplement its power supply.

### ***3.1. Surveys***

Before beginning lab experimentation, Team Piezo obtained Institutional Review Board (IRB) approval to conduct surveys to collect data from smartphone users. The team used the surveys to determine how many times an average college-aged user taps their screen and with what amount of pressure. This data, along with lab data, was used to determine the amount of energy a piezoelectric screen could generate.

#### **3.1.1 Usage Survey**

The usage survey's purpose was to find out how often college students use their smartphones based on their personal assessment and actual data. The team targeted Android users at UMD by posting advertisements in the UMD Facebook group pages.

The team collected data from 25 participants in this survey. At the first meeting, a questionnaire was handed out to the participants asking for various demographic information, such as age and gender. The questionnaire also asked how often they use various phone applications such as messages, Facebook, Twitter, etc. The team then taught the participants how to download the Phone Addict application from the Amazon store. Phone Addict is an application that runs in the background of the smartphone and records how often the user taps the screen (Phone Addict, 2013). After a month, a second meeting was conducted for the team to collect the data from each participant's application.

#### **3.1.2 Pressure Survey**

At the second meeting, the team also tested the force users applied when tapping their smartphones. Participants tapped on Flexi-Force A201 sensors mounted on a Samsung Galaxy S3. The sensors were attached to a Vernier Voltage probe that was connected to a computer running the Vernier data collection software. When the force sensor is unloaded, its resistance is very high. When a force is applied to the sensor, this resistance decreases. The system was calibrated by recording the voltage generated by objects with known weights. The team then determined the relationship between



voltage and force to calculate the force per tap. The team used the results to find the average force used when typing on smartphones.

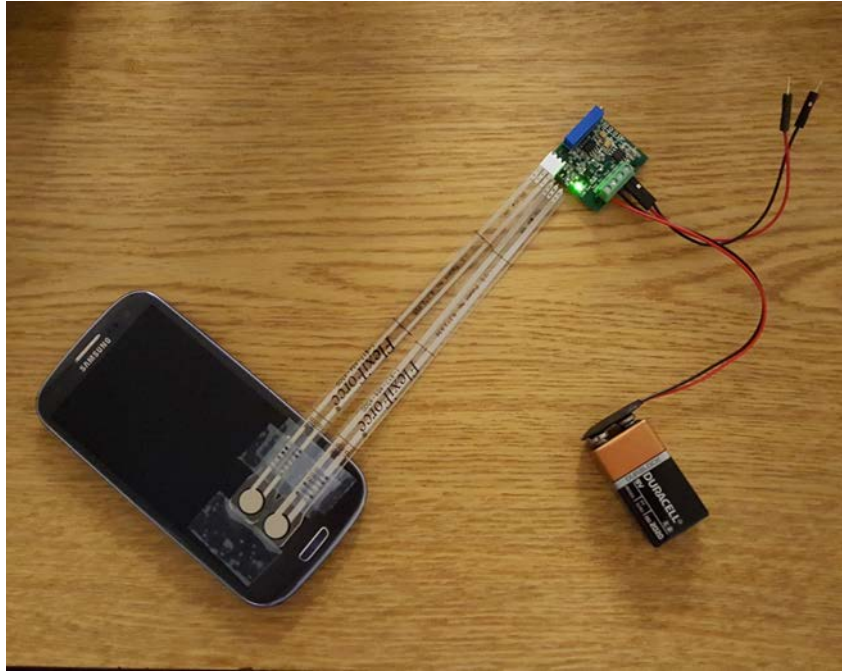


*Figure 8: Data collection apparatus for pressure survey.*

## ***3.2 General Experimentation/Preliminary Testing***

### **3.2.1 Piezoelectric Material Selection**

In order to begin the research to determine the project's feasibility, a piezoelectric material had to be chosen first. A polymer-based film from Emfit was selected for this purpose because it was relatively inexpensive. In addition, the film was partially transparent, which would be required should the film be placed above the LCD layer in a phone screen. The film also required electrodes to be deposited on both sides so that the charge produced when pressed could be collected. To do this, Indium Tin Oxide (ITO) was deposited on the film using the Denton E-beam in the Maryland NanoCenter. Using laser cut acrylic masks, small titanium leads were also deposited on both sides to make effective connections. The preliminary connections were with Wood's metal; however, the metal would not adhere to the electrodes once cooled. The traditional method of soldering connections onto both sides of the film was attempted; however, it was found that the solder melted the film because the temperature was too high. Testing proceeded using aluminum foil for temporary connections since a permanent solution could not be found.

The preliminary tests focused on mechanical features of the film, such as determining the modulus of elasticity of the piezoelectric film. This test was done by fixing the film on one end, placing multiple premeasured paper clips on the open end, and measuring the deformation from the unweighted equilibrium point; this experiment will be described in more detail in Section 3.2.2. The film's electrical properties were

tested as well by connecting the films to an oscilloscope and determining that there was a noticeable spike in voltage once the film was deformed.

The polymer films displayed some positive results but there were many issues that the team was not able to overcome. The film needed to be transparent to be placed on top of the LCD layer. The film itself was not completely transparent, and after ITO was deposited, the film turned completely black. When testing, pieces of foil were used to connect the leads to the film since Wood's metal did not work. However, while testing was still possible, the film itself would not have been a viable material for the final prototype. In addition, after several tests, the films became unresponsive and would no longer produce a voltage signal. Instead of troubleshooting the issues, a new material was found to better fit the team's requirements.

Team Piezo chose to use a PZT-based piezoelectric ceramic from piezo.com for the new material (Figure 9) because it had a more reliable output and was already coated with nickel electrodes. This allowed the team to save time and money as the deposition process was no longer needed. However, because the ceramic was not transparent the touchscreen layer configuration was changed so that the piezoelectric layer would be placed below the LCD layer. The configuration changed some testing procedures but it was a small hindrance and testing proceeded accordingly.



Figure 9: PZT-based piezoelectric ceramic tiles from piezo.com.

Soldered connections were applied to the electrodes, and multiple experiments were conducted with the piezoelectric material. One of the first experiments conducted was determining the ceramic's modulus of elasticity by placing incremental weights on the ceramic and measuring the bending that resulted with each weight; this experiment will be described in more detail in Section 4.2.1. The major disadvantage of using the ceramic piezoelectric tiles is the brittle nature of the material. Over time, the forces applied to the tile result in the formation of small cracks. After a certain amount of fatigue, these cracks propagate and cause brittle failure.

Later in the process the piezoelectric material was etched to create grid segments on the ceramic without completely dividing the full piezoelectric piece; this was done to create separate outputs from different areas on the ceramic material without physically separating the tile into smaller pieces. Sensing capabilities of the ceramic tile were also tested by connecting etched tiles and corresponding LEDs to an Arduino and showing that pressing different segments would light up the respective LEDs.

### 3.2.2 Touchscreen System Modeling

Team Piezo used modulus testing to find the material properties of the polymer piezoelectric films, the ceramic PZT tiles, and the flexible LCD layer in an iPhone 5. The modulus values allowed the team to model the prototype discussed in Section 4.2.1 using FEA. Testing involved placing weights on small sections of the material to model a cantilever system. The procedure varied slightly for each material. However, each method used a cantilever system which could be modeled because it met the following criteria according to Gilbert, 2011:

- The material must be rigid and capable of being parallel to the horizontal plane.
- The material must be in its elastic region of its stress strain curve (Figure 10). To prove a material is in its elastic region after weights are removed, the material must return to parallel to the horizontal plane.
- The material should be in the shape of a rectangle.
- The deflection must be much smaller than the width of the material.
- The material must be fixed on one end and free on another.

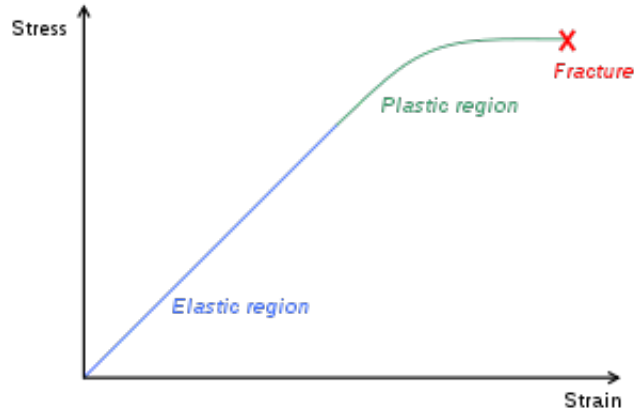


Figure 10: If a material is in the elastic region of its stress strain curve it has not bent far enough to deform its shape. Once a material has entered the plastic portion of its stress strain curve it is permanently deformed. (Wikipedia, 2017)

In addition, standard assumptions were made to simplify calculations. A weight was treated as a point source acting from its center of gravity. A distributed load of an object with a uniformly distributed mass will have the same effect on a cantilever as a force vector at the object's center of mass (Gilbert, 2011). The moment arms ( $a$ ,  $a+b$ ,  $a+b+c$ ) were recorded as the distance to the center of gravity of each mass from the fixed point. Length is the distance from the fixed point to the center of gravity of the largest weight. The max deflection was recorded at the center of gravity of the largest weight. The cantilever model can be seen in Figure 12 (Benham, n.d.). The equations used for the calculations are Equation 1.

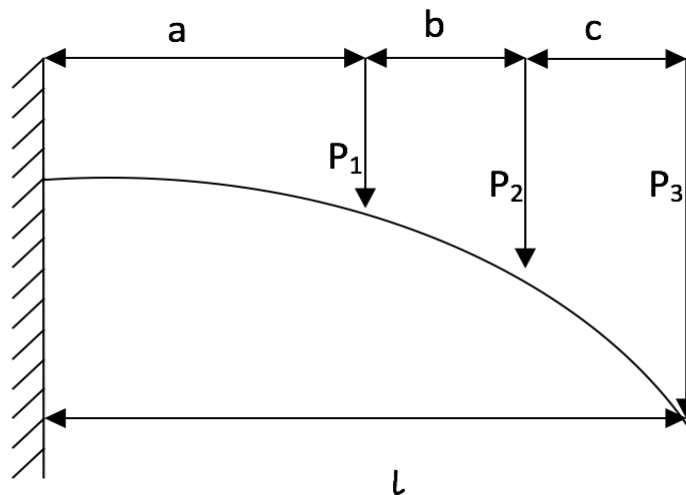


Figure 11: Diagram of cantilever beam dimensions used for modulus testing

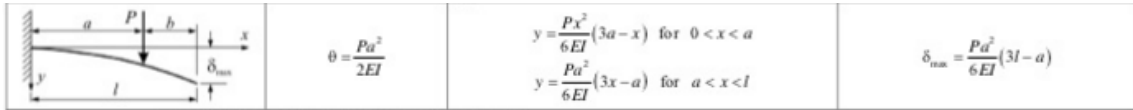


Figure 12: Cantilever model with equations (Benham, n.d.)

Equation 1: Displacement and Modulus of Elasticity equations for cantilever beam

One Weight: Max Deflection ( $\partial$ )

$$= \frac{[\text{Mass} * \text{gravity} * \text{Distance to weight}^2 * [3 * \text{length} - \text{Distance to weight}]]}{[6 * E * \text{Area Moment of Inertia}^4]}$$

One Weight: Modulus of Elasticity (E)

$$= \frac{[\text{mass} * 9.81 * \text{distance to weight}^2 * (3 * \text{length} - \text{distance to weight})]}{[6 * \text{max deflection} * \text{moment of inertia}]}$$

Multiple Weights: Max Deflection ( $\partial$ )

$$= \frac{P_1 * a_1^2 * (3l - a_1)}{6 * E * I} + \frac{P_2 * a_2^2 * (3l - a_2)}{6 * E * I} + \frac{P_3 * a_3^2 * (3l - a_3)}{6 * E * I}$$

Multiple Weights: Modulus of Elasticity (E)

$$= \frac{P_1 * a_1^2 * (3l - a_1) + P_2 * a_2^2 * (3l - a_2) + P_3 * a_3^2 * (3l - a_3)}{6 * I * \partial_{max}}$$

Often, materials that are flexible can be modeled as a cantilever if the specimens are short enough. Decreasing size decreases the length to the force, which decreases the strain on the film by the weight and makes it less likely to permanently deform. The following steps were taken to complete modulus testing.

Materials

- Strip of the Material
- Weights of smaller diameter than the material
- Ruler
- Clamping mechanism for fixed support

Modulus Testing:

1. Make sure the material is cut into a rectangle.
2. Secure the material in the clamping mechanism.
3. Record the initial height of the material.
4. Record the width of the material.
5. Place weight(s) on the cantilever section.
6. Adjust the length so that with a given weight, the material remains suspended.
7. Record the distance to the center of gravity of the weights.



8. Record the applied weight(s).
9. Record the location of the center of gravity of the weights.
10. Repeat steps 6-10 with varied weight.
11. Calculate the modulus.



*Figure 13: Modulus testing apparatus.*

### 3.2.3 Force vs. Voltage

Force vs. voltage gives a picture of the performance of the piezoelectric material under different loading conditions. In order to complete the force vs. voltage testing, a test apparatus was designed, a calibration curve was developed for the Flexi-Force sensor, and tests were performed to get information on the output of the piezoelectrics. The system applied varying measured forces in order to give an accurate picture of piezoelectric responses to different forces.

#### Materials

- Diligent Analog Discovery USB Oscilloscope
- Resistor (10 k $\Omega$ )
- Operational amplifier
- Flexi-Force sensor
- Piezoelectric specimen
- Mounting for force application assembly
- Arduino UNO
- Continuous servo motor
- String
- String guide
- 3-D printed weight holders

- Weight set

### Steps for creating a calibration curve

1. Attach the Flexi-Force sensor to the circuit shown in the Figure 14.
2. Using the Digilent, turn on the -5V and +5V to the operational amplifier and apply a -5V to the input of the Flexi-Force sensor using the Waveforms software.
3. On the oscilloscope screen, click on the Measure button. Add a vertical average value to the measure.
4. One at a time, apply each of the weights in the weight set to the Flexi-Force sensor and measure the average voltage while the weight is applied.
5. Plot each of the average voltages corresponding to their weights in order to get a curve.
6. It should be noted that if tests are not completed on the same day, the calibration curve should be recreated.

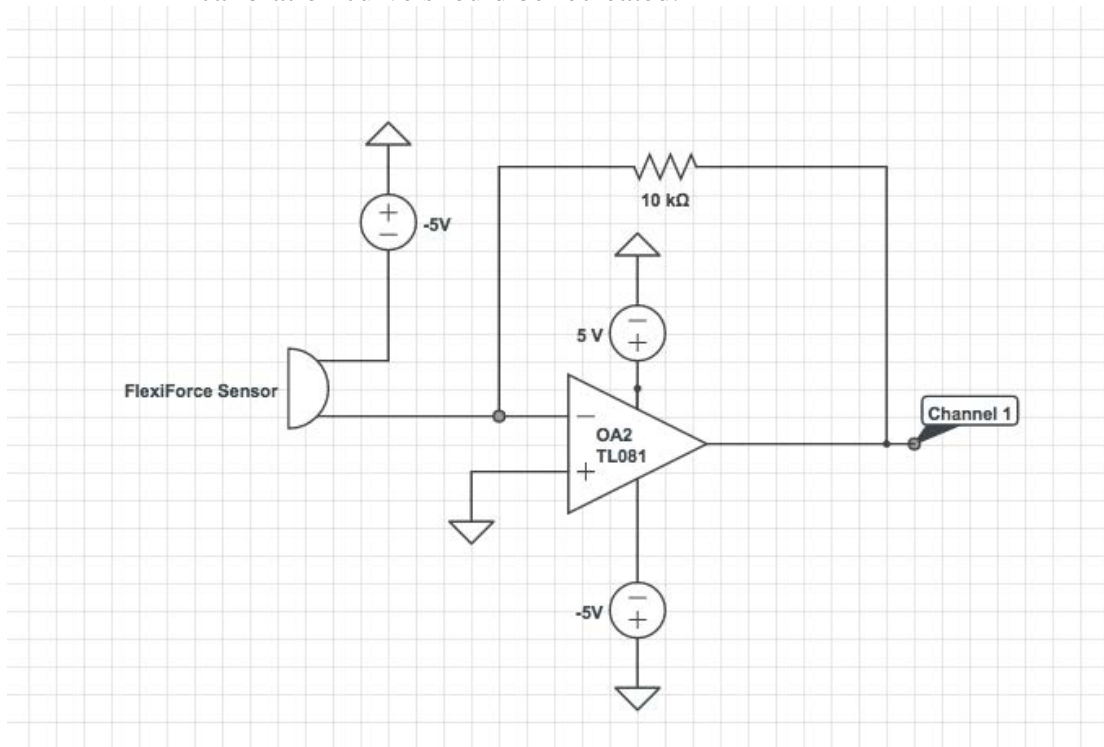


Figure 14: Circuit diagram used to collect data for the calibration curve.

### Steps for setting up the test apparatus

1. Mount the servo motor at an appropriate height above the force sensor.
2. Upload the Arduino code in Figure 7.

```

#include <Servo.h>

Servo myservo;

void setup() {
  // put your setup code here, to run once:
  myservo.attach(3); // attaches the servo on pin 3 to the servo object
}
void loop()
{
  myservo.write(130);
}

```

Figure 15: Servo motor Arduino code for force vs. voltage testing.

4. Attach the string to the servo motor arm.
5. Attach the string guide to the mount and feed the string through.
6. Attach the 3-D printed weight holder with weight to the string.
7. Center the Flexi-Force sensor and/or piezoelectric tile below the weight.
8. Attach the motor to the Arduino's 5V, ground, and digital pins, as shown in Figure 14.

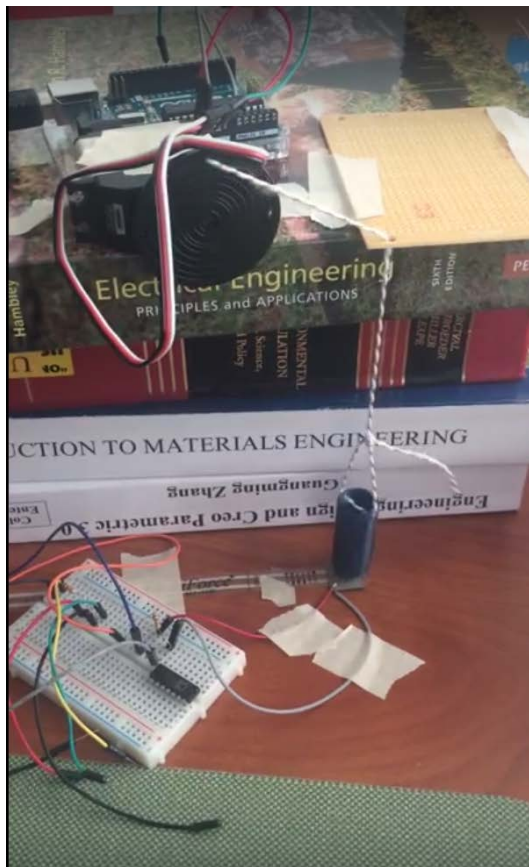


Figure 16: Picture of the apparatus set up for the force vs. voltage data collection.

### Testing the force applied or the piezoelectric voltage produced

1. Set up the test apparatus with the Flexi-Force sensor to calculate force for a given weight set/motor speed or use the piezoelectric tile to collect voltage data, as shown in Figure 17.
2. Run the power, wave generator to power the sensor circuit.
3. Run the oscilloscope to analyze data.
4. Record the peaks at a given speed in the Arduino code with a given weight set.
5. Calculate force from the sensor data using the calibration curve and assign the value to the corresponding piezoelectric voltage data.
6. Repeat the procedure with different speeds in the Arduino code in the myservo.write section and the weights in the test apparatus.

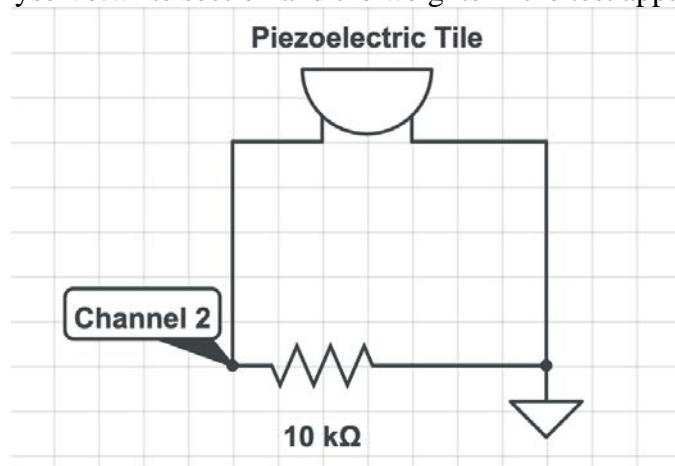


Figure 17: Circuit diagram used for the force vs. voltage data collection.

### 3.3 Circuit Design for Power Storage

In order to charge a battery with the output of a piezoelectric device, it needed to be converted into a constant DC output with a voltage high enough to overcome the voltage rating of the battery itself. Several methods to raise voltage were considered and attempted. Amplifiers were able to raise voltage levels, but required their own power source and as a result the system would consume more power than what was generated. Transformers have also been commonly used in power applications to step up or step down voltage of an AC input. Ideally, the AC output voltage of the piezoelectric device would increase dramatically by a step-up transformer at the ratio of the coils from the input side to the output side. Experiments were done with transformers to attempt this based on the circuits shown in Figure 18.

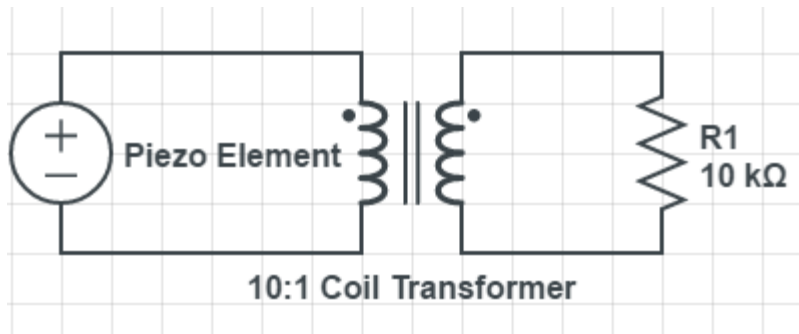


Figure 18: Transformer circuit for voltage step-up. Created in CircuitLab.

Unfortunately, these experiments were unsuccessful; there was no measureable output across the resistor. The piezoelectric element was unable to produce steady AC at the minimum operation frequency for the transformers used in initial testing. The tests were then repeated with the lowest frequency threshold transformers commercially available – as low as 50 Hz. However, the results were the same. Therefore, it was concluded that a step-up transformer was not a viable option for manipulating the output of the piezoelectric device.

The remaining realistic method for accomplishing power storage with the proposed device was to incrementally charge a capacitor with a large number of taps. This would then discharge into a battery by occasionally adding small bursts of energy, which slightly extends the battery life. A capacitor will not charge with an AC wave so any circuits created for this application would need to rectify the output of the piezoelectric element. Once the capacitor is fully charged to the adequate voltage, a switch would connect the capacitor in series with the device battery instead, where it would discharge into the battery, raising its state of charge. This type of charging circuit is unreliable, and risks possible damage to the battery; however, due to design limitations experienced in previous attempts, it was determined to be the most viable. A representative circuit is displayed in Figure 19.

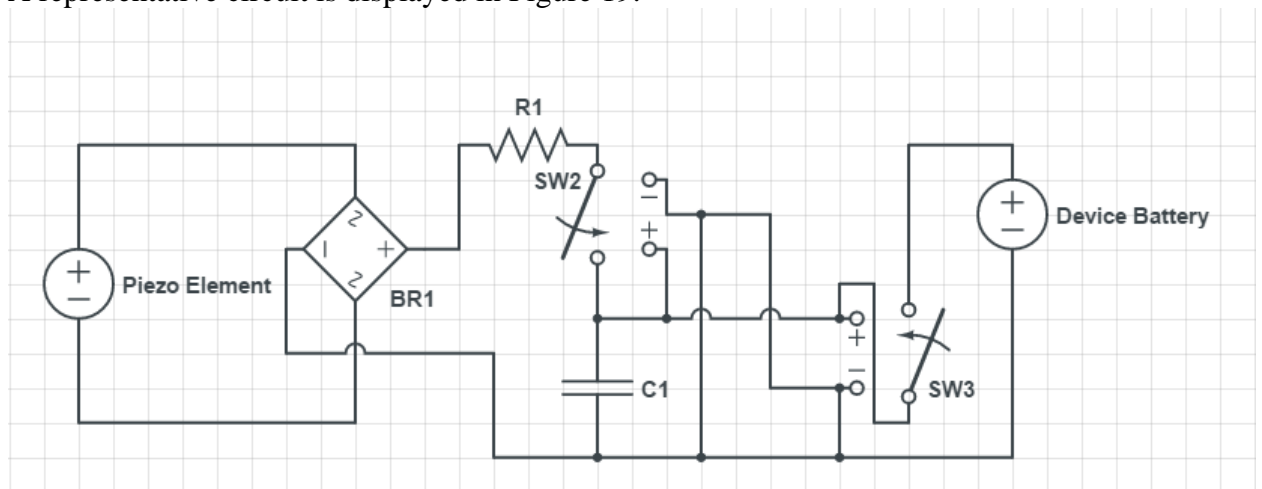


Figure 19: Capacitor-based charging circuit. Created in CircuitLab

In this design, at the desired capacitor voltage difference for C1, both switches would activate, opening the circuit with the resistor and rectifier, and closing the circuit with the device battery. In order to carry out this design, tests were first done with a bridge

rectifier made out of standard diodes in an attempt to charge a capacitor. This was done with a 10nF capacitor in order to charge quickly for the purposes of the experiment. The circuit diagram of the experiment is shown in Figure 20.

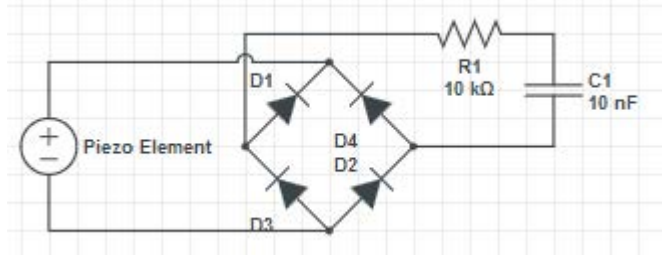


Figure 20: Experimental piezoelectric capacitor charging circuit. Created in CircuitLab

Due to the low voltage of the input signal, the voltage drop across the diodes (700 mV is standard) could not be overcome, there was no measurable output signal, and the capacitor could not be charged.

Further experiments were done with advanced diodes with extremely low voltage drops of approximately 50 mV. Diodes with even lower voltage drops were researched, but were commercially unavailable, and thus not an option. The same bridge rectifier experiment was repeated with the low voltage diodes, as well as an additional experiment with a half-wave rectifier. A circuit diagram of the half-wave rectifier experiment is shown below.

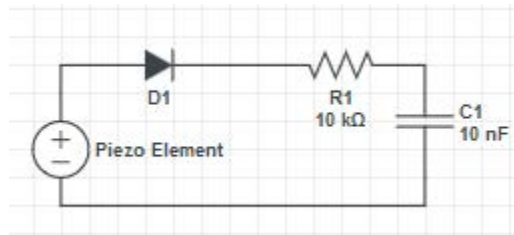


Figure 21: Half-wave rectifier experimental capacitor charging circuit. Created in CircuitLab

A half-wave rectifier is a diode in series with the rest of the circuit; it does not produce a positive output when the input signal is negative like a full-wave bridge rectifier would. However, the diode blocks any negative current, preventing negative voltages which would otherwise be forcibly discharging the capacitor. The advantage of the half-wave rectifier is that the signal only passes through one diode instead of two, which can be advantageous in situations where the input voltage is very low. Unfortunately, due to the failing results of the capacitor experimentation, as well as time constraints on the project, further variations of these circuits were not tested, and the goal of power generation could not be fully explored.

### 3.4 Prototype

#### 3.4.1 Grid Design

The basis for Team Piezo’s touchscreen prototype design was to split a piezoelectric element into several segments arranged in a grid. Because each segment

was electrically isolated, the location of an applied force could be determined based on the voltages produced by the activated segments. Over the course of the research process, two main prototype designs were considered using either physically separated elements or a single element with electrical separation in the electrode layer.

The first prototype concept featured a grid of physically separated piezoelectric segments (Figure 22). The ceramic piezoelectric material was cut using the Microautomation dicing saw (typically used for cutting silicon wafers) in the Maryland NanoCenter. This equipment allows the fragile material to be cut precisely without causing brittle fracture, which is a typical failure mode for ceramic materials. A separate mounting grid was fabricated using 3-D printing. For the initial prototypes, soldered connections leading to separate analog microcontroller inputs would be made to both sides of each piezoelectric segment. The connections were made using lead-free solder and Superior No.30 Halide flux.

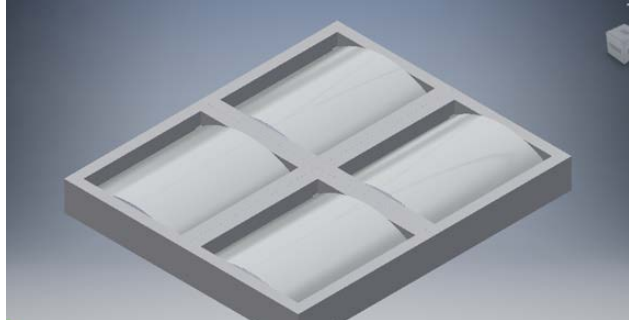


*Figure 22: Physically separated grid section prototype concept.*

The second prototype design involved creating electrical separation to form the grid pattern without physically dividing the piezoelectric element. Because the voltages were read exclusively from the nickel electrodes deposited on both sides of the ceramic, it was possible to create the grid segments by only removing material from the electrode layer on both sides of the tile. In order to control deformation and provide repeatable feedback results, a laser-cut acrylic mounting grid was used to support the piezoelectric tile (Figure 23). The lack of physical separation caused a larger section of the piezoelectric element to be activated by an applied force, so more energy could theoretically be generated and collected. In addition, the lack of plastic grid members between segments reduced the amount of wasted space in the touchscreen.



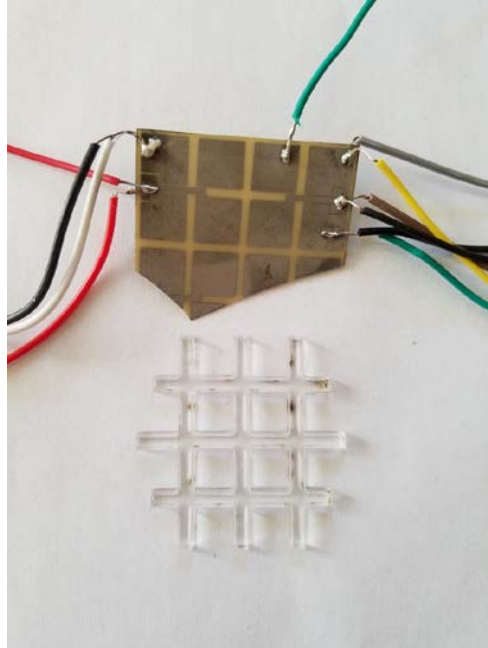


*Figure 23: A fractured piece of a 4x4 etched piezoelectric prototype with an acrylic mounting grid*

The prototype was fabricated by etching the nickel electrodes in the Maryland NanoCenter. This process involved briefly submerging the tile in a heated chemical etchant to remove part of the electrode layer. Photoresist was used to protect most of the surface from the etchant. For the initial test piece, the photoresist was simply painted on both sides leaving a strip down the middle. For more complicated patterns, the entire surface was coated. Then, a printed mask was placed on the surface, and UV exposure deactivated the unmasked sections of photoresist. The entire lab procedure for fabricating the grids is presented in the following paragraphs.



*Figure 24: Two part etched piezoelectric element for initial testing/proof of concept*



To begin, the desired pattern for both sides was drawn in CAD. The mask's pattern divided the electrode layer into square sections. Interior segments were routed to the outside for soldering using thin strips of the electrode. Then, the drawing was opened in Adobe Illustrator to develop a PDF with the correct sections filled in. A standard inkjet printer was used to transfer the pattern to a transparency sheet. A second layer of ink was needed to make the pattern opaque enough to protect the electrode from the UV light exposure for the etching process. Several attempts were required to minimize the offset of the second layer and ensure that the channels remained clear. As the etching pattern becomes more intricate with smaller grid segments in future research, printer accuracy limitations may necessitate having a mask printed professionally.

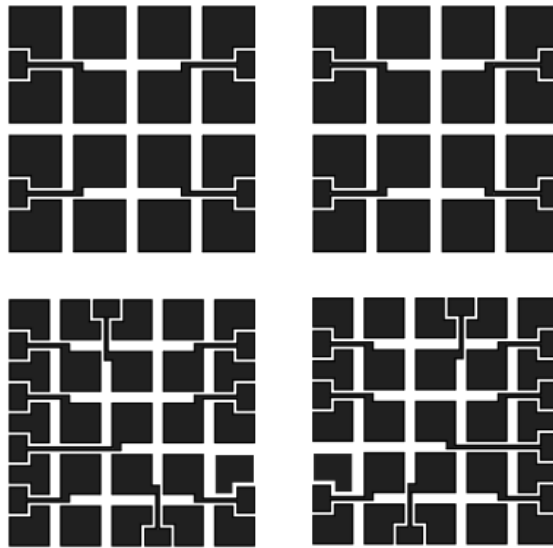


Figure 25: Front and back mask designs for 4x4 and 5x5 grids

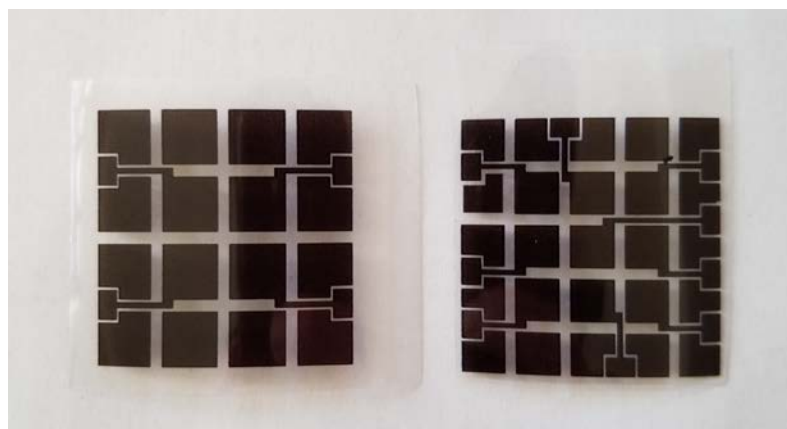


Figure 26: Printed masks, one side of 4x4 and 5x5 grids

The etching process in the Maryland NanoCenter began by solvent cleaning the piezoelectric element in a wet bench to remove particulates. The solvent clean consisted

of spraying the tile with wash bottles of acetone, methanol, isopropyl alcohol, and distilled water. The surface was dried with pressurized nitrogen gas. Placing the tile on a 120-degree Celsius hot plate for a minimum of two minutes removed any remaining moisture. The first electrode surface was prepared for photoresist by coating it in HMDS and spinning (Headway EC-101 spin station) for 40 seconds at 4000 rpm. This step improved the photoresist adhesion since it would be face down on a hot plate while coating the opposite side. Next, the surface was coated in 1813 positive photoresist and spun for a complete cycle to achieve a 1.4-micron layer. The tile was placed on a 100-degree Celsius hot plate for one minute to cure the photoresist. This process was repeated without HMDS for the second electrode surface.

The mask was cleaned by spraying it with a wash bottle of isopropyl alcohol and dried with pressurized nitrogen gas. A Karl Suss MJB-3 Mask Aligner was used for the UV exposure. This involved placing the piezoelectric element on the chuck and carefully aligning the mask ink side down on the electrode surface by hand. Then, the chuck was pressed into a clear glass mask beneath the lamp. A 5.5 second 365 nm UV exposure at 8 mW/cm<sup>2</sup> deactivated the exposed photoresist. The photoresist was developed with Microchem CD26 developer (metal ion free) for 40 seconds to one minute. When all of the features were visible, the tiles were dehydrated on the 120-degree Celsius hot plate for at least 2 minutes to ensure the photoresist adhered to the electrode surface. In a wet bench, the tile was submerged in 40-degree Celsius nickel etchant until the exposed sections of electrode were entirely removed and the color of the ceramic was revealed. The etched tile was finished with another solvent clean. The acetone was used to remove the remaining photoresist.



*Figure 27: Full 5x5 etched piezoelectric prototype grid*

### 3.4.2 Voltage, Power, Waveform Characteristics

Understanding the characteristics of the voltage waveform produced by tapping a piezoelectric tile was necessary to develop a prototype. Because the deformation caused by a tap is not confined to a single grid segment, the waveform differences caused by direct versus indirect taps had to be identified for use in the location sensing algorithm. This section will cover tests performed on the unaltered piezoelectric tile, the proof of concept etched tile, and the prototype etched grids.

In order to gain insight into the electrical properties of the ceramic tile, the team observed the voltage patterns that resulted from tapping the material. The voltage was measured across a  $10\text{k}\Omega$  resistor using a Digilent Analog Discovery USB oscilloscope to display the waveforms being produced. The circuit shown in Figure 28 was used to gather data from the unaltered piezoelectric tile.

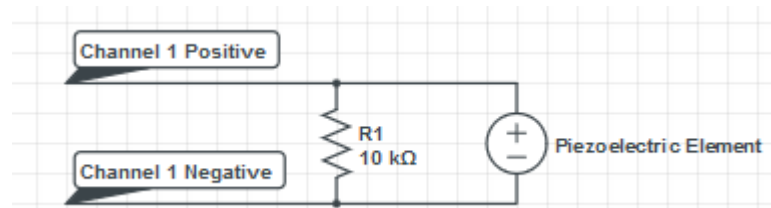


Figure 28: Circuit for measuring voltage waveforms with one piezoelectric element. Created in CircuitLab.

As further design decisions were made with regard to the method of piezoelectric sectioning, additional testing was implemented to evaluate the fundamentals of the design. The proof of concept two-segment, etched, piezoelectric tile was tested with the same methods, but the voltage waveforms of both tile sections were measured independently (Figure 29).

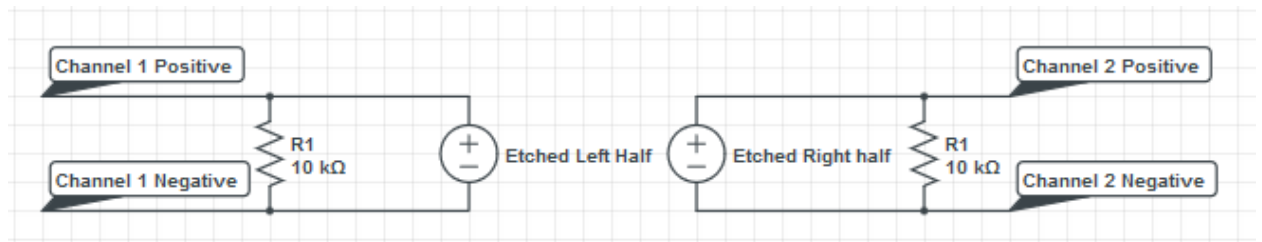


Figure 29: Circuit for measuring voltage waveforms with two piezoelectric elements. Created in CircuitLab.

This was done in order to compare the waveforms resulting from the directly tapped sections and the adjacent section. For example, it was expected that a direct tap to a specific segment of the tile would result in a higher voltage peak and a slightly earlier spike.

The prototype etched grids were tested using the same circuit connected to various grid segment combinations. For this test, the piezoelectric tile was mounted on a laser cut grid to improve consistency of the response and to provide some physical isolation between grid elements.

### 3.4.3 Arduino Prototype

Initial testing of the etched piezoelectric element was conducted using Digilent Analog Discovery USB Oscilloscope. Based on observations from these tests in Section 4.4 a prototype (Figures 30, 31) was developed using an Arduino UNO microcontroller. An Arduino code was written to continuously collect voltage data through the analog pins. An algorithm monitored the data for certain patterns in the waveform and triggered an output through the Arduino's digital pins to light up LEDs corresponding to the various sections. The prototype code will be explained in detail in the following paragraphs.

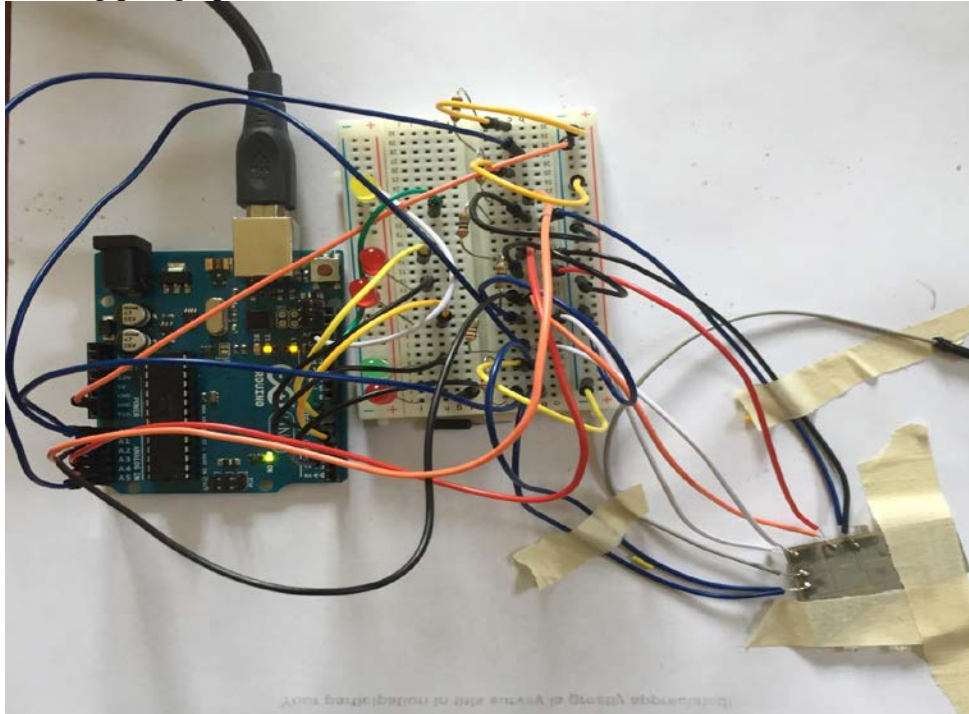


Figure 30: Prototype testing setup.

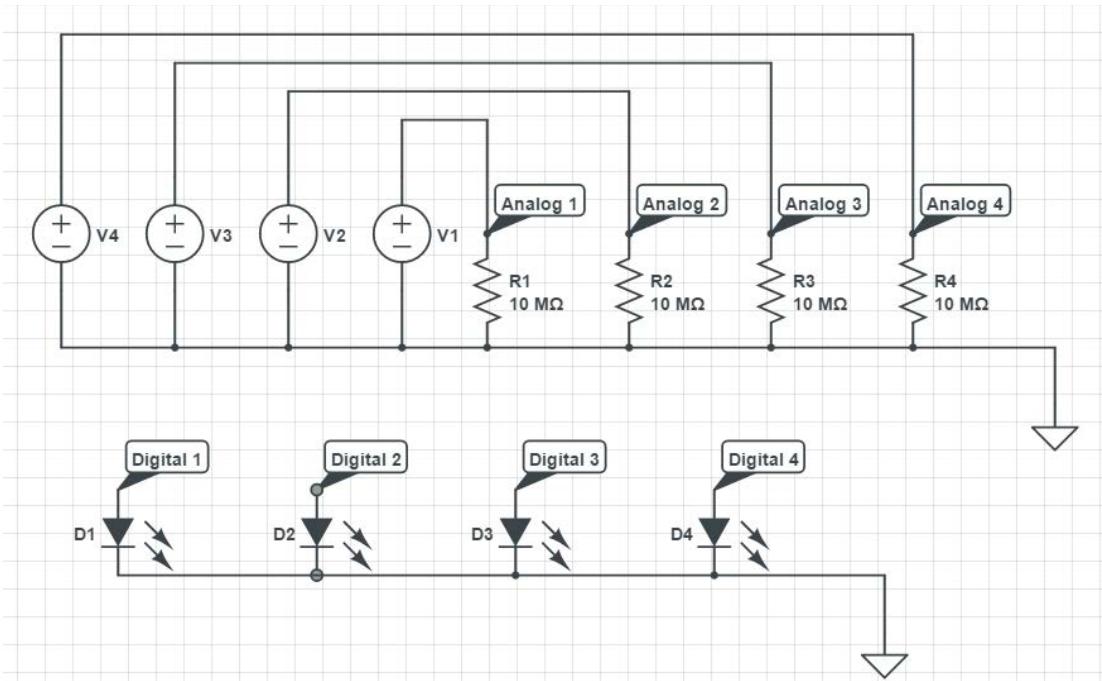


Figure 31: Prototype testing setup circuit diagram. Voltage sources represent piezoelectric grid sections. Created in CircuitLab.

In the setup function, serial communication was established at a baud rate of 115200. Several variables were defined at the beginning of the loop function. A multidimensional array for buffering waveform data contained 50 rows of data with columns for each segment of the grid. Variables for storing the maximum analog value and the corresponding column were defined, and the digital pins for the LEDs were set to output mode (Figure 32).

```
void setup() {
  // put your setup code here, to run once:
  Serial.begin(115200);
}

void loop() {
  // put your main code here, to run repeatedly:

  int data[50][6];
  int data_max = 0;
  int location;
  pinMode(7, OUTPUT);
  pinMode(2, OUTPUT);
  pinMode(3, OUTPUT);
  pinMode(4, OUTPUT);
  pinMode(5, OUTPUT);
  pinMode(6, OUTPUT);
}
```

Figure 32: Arduino code setup and variable declaration.

The data array was initially filled using the `analogRead()` function in a for loop that ran 50 times (chosen arbitrarily) at the beginning of the code. The remaining commands were placed in a `while(1)` loop to run continuously. First, nested for loops were used to move the value in each element up one row. Then, the last row was filled with new data that included multipliers to account for variability of the voltage output of different segments (Figure 33).

```

for(int i=0; i<50; i++){
  float segment1 = analogRead(A0);
  float segment2 = analogRead(A1);
  float segment3 = analogRead(A2);
  float segment4 = analogRead(A3);
  float segment5 = analogRead(A4);
  float segment6 = analogRead(A5);
  data[i][0] = segment1;
  data[i][1] = segment2;
  data[i][2] = segment3;
  data[i][3] = segment4;
  data[i][4] = segment5;
  data[i][5] = segment6;
}

while(1){
  for(int i = 0; i < 49; i++){
    for(int j = 0; j < 6; j++){
      data[i][j] = data[i+1][j];
    }
  }

  float segment1 = 1.4*analogRead(A0)
  float segment2 = 7.4*analogRead(A1)
  float segment3 = 1.95*analogRead(A2)
  float segment4 = .75*analogRead(A3)
  float segment5 = analogRead(A4);
  float segment6 = analogRead(A5);

  data[49][0] = segment1;
  data[49][1] = segment2;
  data[49][2] = segment3;
  data[49][3] = segment4;
  data[49][4] = segment5;
  data[49][5] = segment6;
}

```

*Figure 33: Arduino code filling the data set and continuously updating data.*

The maximum value variable was reset to zero to clear any residual information from the previous iteration of the continuous loop. Then, an if statement nested in a for loop checked each new data value and chose the largest. If this value exceeded a threshold chosen by analyzing serial data in a separate code, then the remaining code was executed. Otherwise, the code would loop back to read new voltages (Figure 34).

```

data_max = 0;
Serial.println(data_max);
for(int i=0; i< 6; i++){
  if(data[49][i] > data_max){
    data_max = data[49][i];
  }
}

```

Figure 34: Arduino code selecting maximum value from new voltage data.

Assuming the maximum value exceeded the threshold, an identical set of loops would replace the entire data set with new data to capture the rest of the waveform from the piezoelectric element. During this process, the maximum data variable would continue to update, and the location variable would record the column number associated with the current maximum value. This location was used to trigger an LED using the digitalWrite() and delay() commands (Figure 35).

```

if(data_max>40){

  for(int i = 0; i <50; i++){
    float segment1 = 1.4*analogRead
    float segment2 = 7.4*analogRead
    float segment3 = 1.95*analogRea
    float segment4 = .75*analogReac
    float segment5 = analogRead(A4)
    float segment6 = analogRead(A5)

    for(int i = 0; i < 50; i++){
      for(int j = 0; j < 6; j++){
        data[i][j] = data[i+1][j];
      }
    }
    data[49][0] = segment1;
    data[49][1] = segment2;
    data[49][2] = segment3;
    data[49][3] = segment4;
    data[49][4] = segment5;
    data[49][5] = segment6;

    for(int j = 0; j < 6; j++){
      if(data[49][j] > data_max){
        data_max = data[49][j];
        location = (j+2);
      }
    }
  }
  digitalWrite(location, HIGH);
  delay(100);
  digitalWrite(location, LOW);
}
}

```

Figure 35: Arduino code identifying a peak, reading remaining waveform, and blinking LED.

## Chapter 4: Results and Discussion

### 4.1 Surveys

The average taps per day for each user was calculated by taking the average of the taps per day collected by the Phone Addict application. From this data, an average was taken to calculate a total average number of taps per day. This average was  $4,745 \pm 2,196$  taps per day. The distribution of these averages is shown in Figure 36.

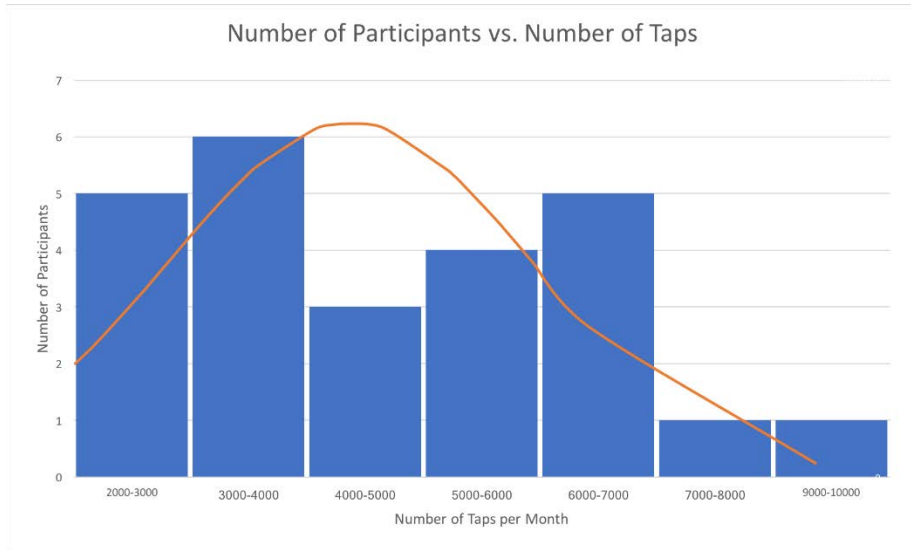


Figure 36: Bar graph showing the distribution of users within the average numbers of taps per month.

The data collected from the Pressure Survey recorded the voltage of the force sensors every hundredth of a second for 15 seconds. For each dataset, a five-point moving average was used to remove sensor noise. This was accomplished by outputting the filtered voltage at time  $t$ ,  $V(t)$ , as an average of the voltages from time  $t-2$  through time  $t+2$ , or  $V_{filtered}(t) = \frac{\sum_{t-2}^{t+2} V_{actual}(t)}{5}$ . A threshold was also applied to the data since values for the sensor were erratic near 0V. Once the data was filtered, voltage peaks were more visible and were counted for our calculations to find an average force per tap. Voltage peaks of the filtered data were found by calculating the slope at each data point; if the slope from one point to the next was negative and the slope from the previous point to the current point was positive, the point was labelled as a local maximum. Once the location (coordinates  $(t_{peak}, V(t_{peak}))$ ) of the local maxima was determined from the filtered data, the true voltage value was located by looking up the actual voltage at that time  $t_{peak}$ . Figure 37 shows a graph of a participant's force data:



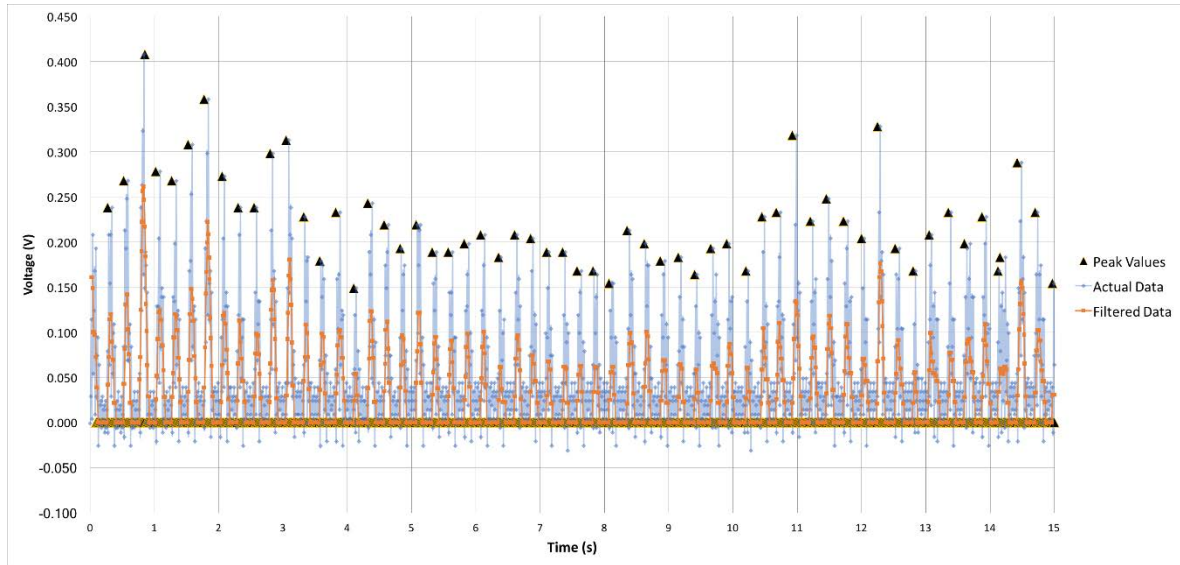


Figure 37: Sample data for Participant 10 with filter.

For each dataset, the average was taken of the maximum peak values. The sensor was calibrated by using known weights and recording the voltage outputted, thus the relationship between voltage and force was known:

$$Force = 0.3456 * Voltage + 0.0502$$

Subsequently, the average was taken for the average force from each dataset. The final average force was  $0.073 \pm 0.018$  N.

This resulting data can determine the desired power output after incorporated figures for the goals of the device. One goal regarding a general energy generation over a day is 2 watt hours, as this is the equivalent of 10% of an iPhone battery (Apple, 2017). The second goal refers to an emergency in which a user would need .1 watt hours to make a 10 minute phone call (Carroll and Heiser, 2010). In the time-unurgent emergency, a user could spend 10 minutes to apply 10,000 high-intensity (1N) taps. Equation 2 below displays the above information.

Equation 2: Power Generation Goals from Survey

$$\frac{5000 \text{ Taps}}{1 \text{ Day}} * \frac{.1 \text{ N}}{1 \text{ Tap}} * \frac{? \text{ Wh}}{.1 \text{ N}} = \frac{2 \text{ Wh}}{1 \text{ Day}}$$

$$\frac{.1 \text{ Wh}}{1 \text{ Call}} * \frac{1 \text{ N}}{? \text{ Wh}} * \frac{1 \text{ Tap}}{1 \text{ N}} = \frac{10,000 \text{ Taps}}{1 \text{ Call}}$$

Equation 2 then offers two goal values for the energy generation. Ideally, the touchscreen will generate .0004 watt hours per tap to satisfy the daily energy goal and .00001 watt hours per high-intensity tap for the emergency-situation goal.

## 4.2 General Experimentation/Preliminary Testing

### 4.2.1 Piezoelectric Material Selection

Based on the reliability problems associated with collecting data from the piezoelectric films from Emfit, Team Piezo chose to use a more reliable ceramic piezoelectric material from piezo.com.

### 4.2.2 Touchscreen System Modeling

Calculating the modulus of the piezoelectric material and LCD screen was necessary to model the physical response of the system. Using the steps outlined in Section 3.2.2 the modulus of three materials was measured.

#### Modulus of the LCD Screen

Table 2: LCD screen properties.

	Thicknesses	Width	Moment of Inertia (m <sup>4</sup> )
mm	1	54	
m	0.001	0.054	4.5E-12

Table 3: LCD screen modulus testing data.

Original height	Final Height	$\delta$	Total Length	Weight 1	Weight 2	a	Weight 3	b	Moment of Inertia	Modulus (Pa)
0.035	0.035	0	XX	XX	XX	XX	XX	XX	4.5E-12	XX
0.035	0.034	0.001	0.015	0.005					4.5E-12	1,250,000
0.035	0.032	0.003	0.015	0.01					4.5E-12	833,000
0.035	0.03	0.005	0.022	0.005	0.01	0.01			4.5E-12	1,200,000
0.035	0.031	0.004	0.017	0.02					4.5E-12	1,820,000
0.035	0.028	0.007	0.024	0.005	0.02	0.011			4.5E-12	1,510,000
0.035	0.027	0.008	0.026	0.01	0.02	0.012			4.5E-12	2,510,000
0.035	0.025	0.01	0.031	0.005	0.01	0.019	0.02	0.006	4.5E-12	2,320,000
0.035	0.024	0.011	0.033	0.01	0.01	0.019	0.02	0.006	4.5E-12	3,620,000
0.035	0.03	0.005	0.024	0.05					4.5E-12	10,200,000
0.035	0.034	0.001	0.012	0.005					4.5E-12	640,000
0.035	0.034	0.001	0.013	0.01					4.5E-12	1,630,000
0.035	0.033	0.002	0.023	0.01	0.005	0.011			4.5E-12	5,200,000
0.035	0.033	0.002	0.015	0.02					4.5E-12	2,500,000

0.035	0.033	0.002	0.025	0.02	0.005	0.012			4.5E-12	12,400,000
0.035	0.032	0.003	0.026	0.02	0.01	0.012			4.5E-12	9,900,000
0.035	0.031	0.004	0.029	0.02	0.01	0.014	0.005	0.003	4.5E-12	10,400,000
0.035	0.03	0.005	0.03	0.02	0.01	0.016	0.01	0.004	4.5E-12	9,510,000
0.035	0.0305	0.0045	0.017	0.05					4.5E-12	4,040,000

Table 4: LCD screen modulus of elasticity results.

Average Modulus of Elasticity 90%	Average	Median	Standard Deviation	Standard Deviation 90%
4,083,000	4,520,000	2,504,000	4,001,856	3,329,661.69

A modulus of 4.08 MPa indicates a very flexible material. This is a positive sign for the model as it increases the amount of force which can be translated to the piezoelectric device. The computer model with the LCD screen was never able to be realized; however, in future work knowing the modulus of all the components above the piezoelectric system will allow the prototype to be accurately modeled.

### Modulus of the Piezoelectric Tile

Table 5: Piezoelectric tile modulus of elasticity results.

	Mass 1	Distance 1	Mass 2	Distance 2	Length	Moment of Inertia	Deflection	
Test 1	0.02	0.0194875	0		0.0269875	1.73E-14	0.0016764	
Test 2	0.02	0.02425	0		0.03175	1.73E-14	0.0018034	
Test 3	0.005	0.0283375	0		0.0333375	1.73E-14	0.0006223	
Test 4	0.01	0.007575	0.02	0.021075	0.0381	1.73E-14	0.0050673	
Device broke after about 30 seconds of loading recorded for yield strength								
Test 5	0.05	0.0286	0		0.0381	1.73E-14	0.0076454	

$$E = \frac{[.05 * 9.81 * (0.0286)^2 * (3 * .0381 - .0286)]}{6 * 1.76264 * 10^{-14} * 0.0076454}$$

$$E = 552964304687 \text{ Pa}$$

	Modulus (Pa)	Modulus (Gpa)
Test 1	26377854415	26.37785442
Test 2	43852675428	43.85267543

Test 3	43796287790	43.79628779
Test 4	16621914112	16.62191411
Device broke after about 30 seconds of loading recorded for yield strength		
Test 5	43416919864	

Table 6: Statistical analysis of modulus of elasticity for piezoelectric tile.

Average	Median	Standard Deviation
32,662,182,936	34,365,678,500	13,490,470,983

$5.2 * 10^{10} = 52,000,000,000$  modulus given by the website

$$H_0 E = 5.2 * 10^{10} Pa$$

$$H_a E \neq 5.2 * 10^{10} Pa$$

Two tailed T hypothesis test

$$t = \frac{\bar{X} - \mu}{S/\sqrt{n}} = \frac{(3.266 - 5.2)^1}{1.349/\sqrt{4}} \quad d.f. = 3$$

$$t = -2.867$$

$$\alpha = .1 \text{ two tailed test } P = .05$$

Since  $-2.8672 > -3.182$  (where  $-1.729$  is the t value corresponding to the chosen alpha value), the team concluded that the manufacturer's value for the modulus of elasticity could be used for simulation analysis seen in Section 4.2.3.

### Finite Element Analysis Simulation

Team Piezo performed Finite Element Analysis (FEA) simulations using Creo Parametric 3.0 in order to understand the stress and strain the ceramic will undergo when the force of one tap is applied to the screen. The simulation was conducted on a model representative of the 4x4 etched tile used in prototype testing. The material properties provided by the manufacturer were used in the model. A force of 0.073N found as the average maximum force applied by users from the surveys was applied as a distributed load across a circular surface area with a diameter of 16mm. This diameter was also used in the team's experimental force vs. voltage testing to represent the size of the average human thumb.

### Corner Mounting

In the first set of analyses, the model was constrained by a 1mm x 1mm square area at each of the four corners on the bottom face, in order to test the team's initial mounting idea. The simulation was run with the force applied in a few different

locations to give the team a comprehensive understanding of multiple loading conditions.

First, the load was centered on one of the etched grid segments, as shown in Figure 38.

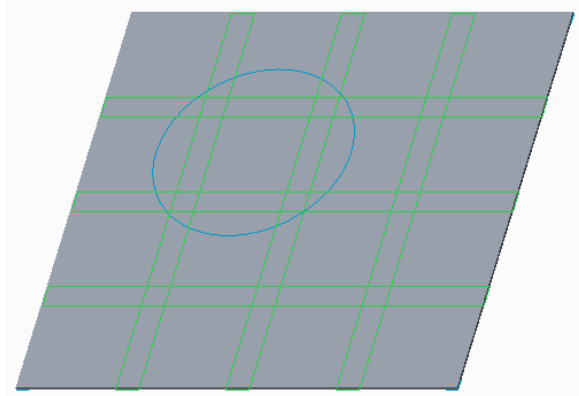


Figure 38: FEA model with load centered on a grid segment.

The results were collected for the von Mises stress distribution (Figure 39) and the maximum principal strain distribution (Figure 40).

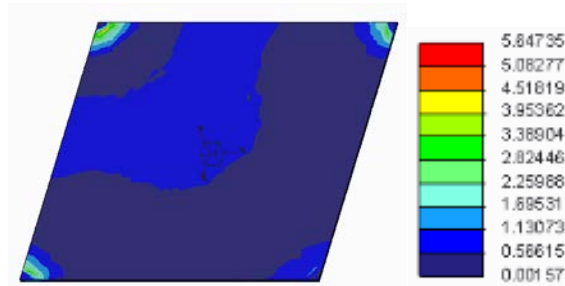


Figure 39: Von Mises stress distribution with load centered on a grid segment; units in MPa.

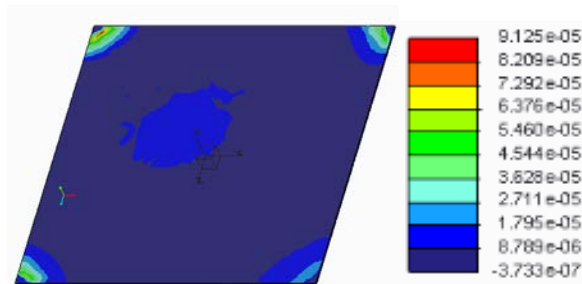


Figure 40: Maximum principal strain distribution with load centered on a grid segment; units in mm/mm.

Next, the load was centered on the tile, which coincided with an intersection of the etching, as shown in Figure 41.

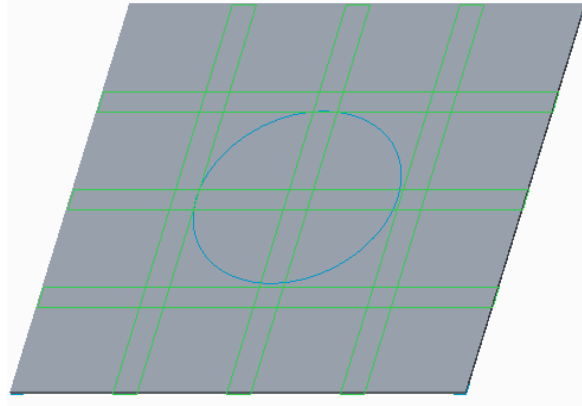


Figure 41: FEA model with load centered on the tile.

The results were collected for the von Mises stress distribution (Figure 42) and the maximum principal strain distribution (Figure 43).

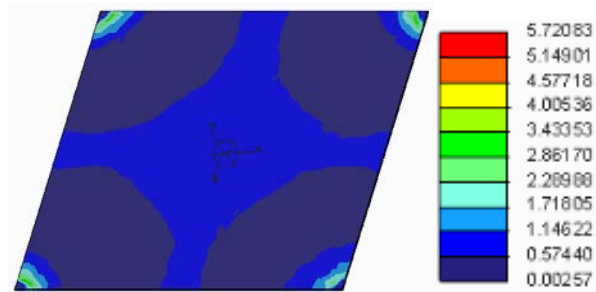


Figure 42: Von Mises stress distribution with load centered on the tile; units in MPa.

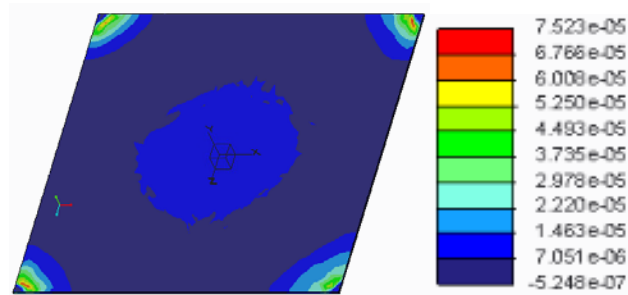


Figure 43: Maximum principal strain distribution with load centered on the tile; units in mm/mm.

A simulation was run when the load was applied on the edge of the tile, as shown in Figure 44.

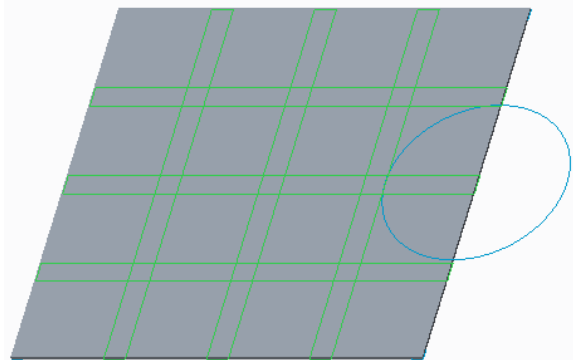


Figure 44: FEA model with load centered on the edge of the tile.

The results were collected for the von Mises stress distribution (Figure 45) and the maximum principal strain distribution (Figure 46).

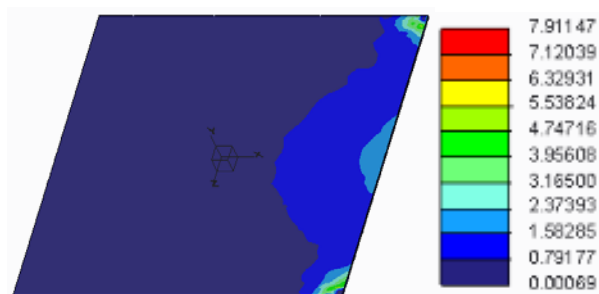


Figure 45: Von Mises stress distribution with load centered on the edge of the tile; units in MPa.

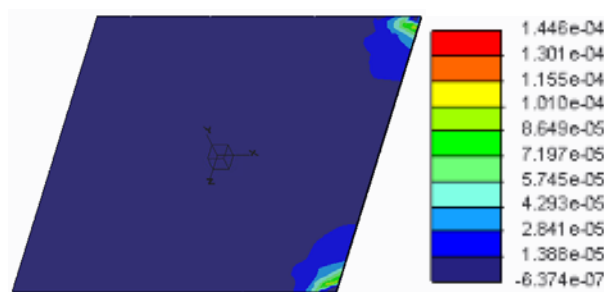


Figure 46: Maximum principal strain distribution with load centered on the edge of the tile; units in mm/mm.

A simulation was run when the load was applied on the corner of the tile, as shown in Figure 47.

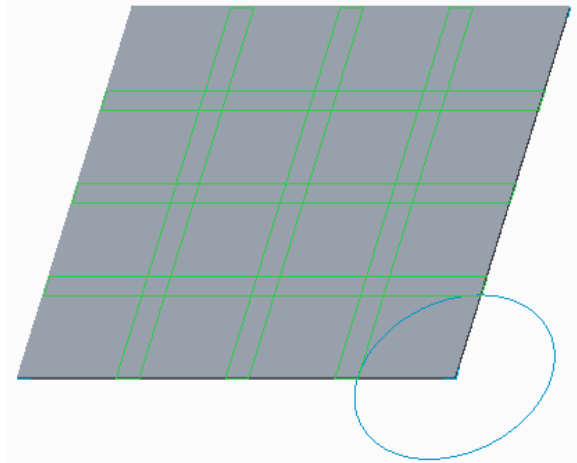


Figure 47: FEA model with load centered on the corner of the tile.

The results were collected for the von Mises stress distribution (Figure 48) and the maximum principal strain distribution (Figure 49).

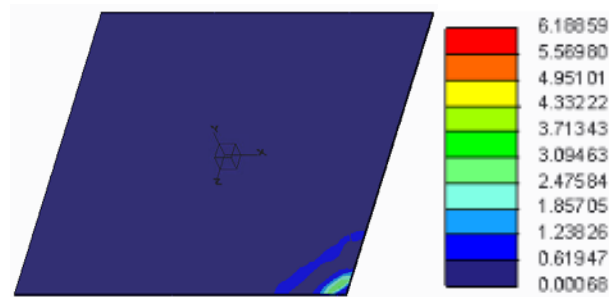


Figure 48: Von Mises stress distribution with load centered on the corner of the tile; units in MPa.

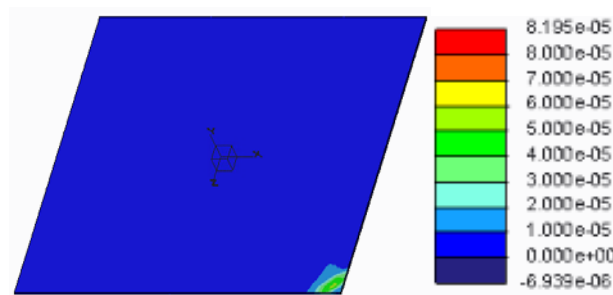


Figure 49: Maximum principal strain distribution with load centered on the corner of the tile; units in mm/mm.

### Grid Mounting

In the second set of analyses, the model was mounted on top of a model of the laser-cut grid. The simulation was run with the force applied in the same locations as the first analyses to allow the team to compare the scenarios directly with different mounting conditions.

First, the load was centered on one of the etched grid segments, as shown in Figure 50.



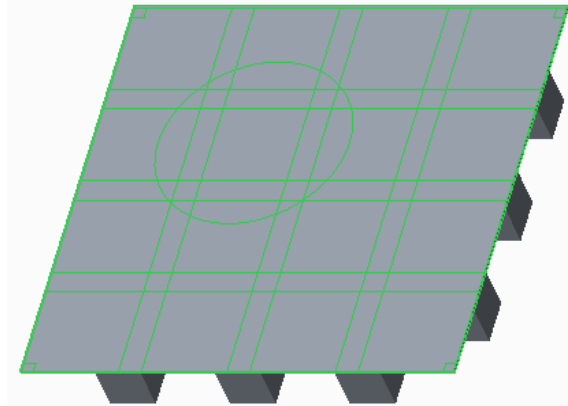


Figure 50: FEA model with grid mounting and load centered on grid segment.

The results were collected for the von Mises stress distribution (Figure 51) and the maximum principal strain distribution (Figure 52).

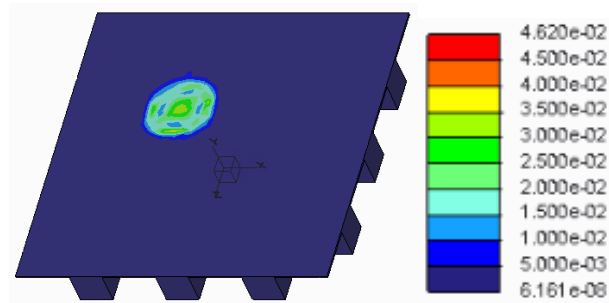


Figure 51: Von Mises stress distribution with grid mounting and load centered on a grid segment; units in MPa.

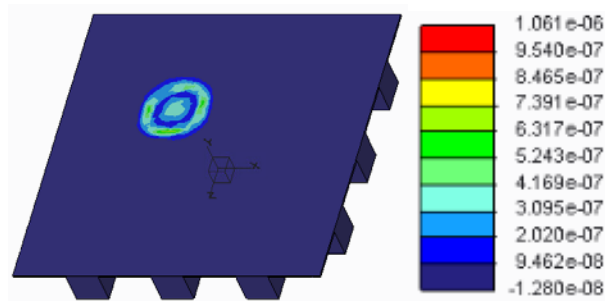


Figure 52: Maximum principal strain distribution with grid mounting and load centered on a grid segment; units in mm/mm.

Next, the load was centered on the tile, as shown in Figure 53.

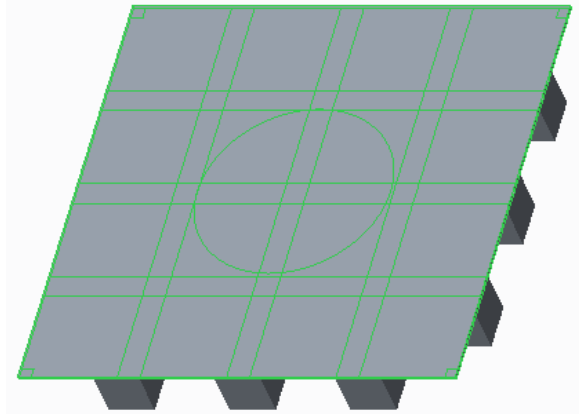


Figure 53: FEA model with grid mounting and load centered on the tile.

The results were collected for the von Mises stress distribution (Figure 54) and the maximum principal strain distribution (Figure 55).

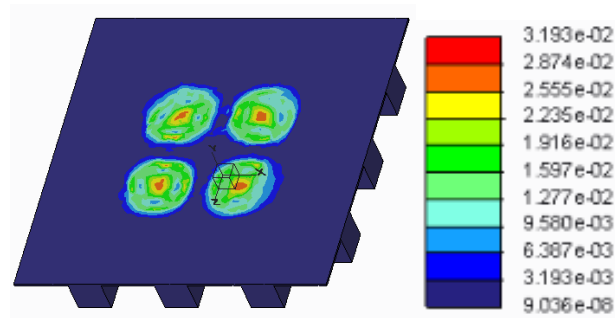


Figure 54: Von Mises stress distribution with grid mounting and load centered on the tile; units in MPa.

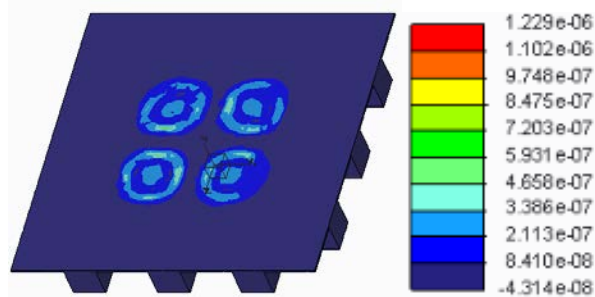


Figure 55: Maximum principal strain distribution with grid mounting and load centered on the tile; units in mm/mm.

A simulation was run when the load was applied on the edge of the tile, as shown in Figure 56.

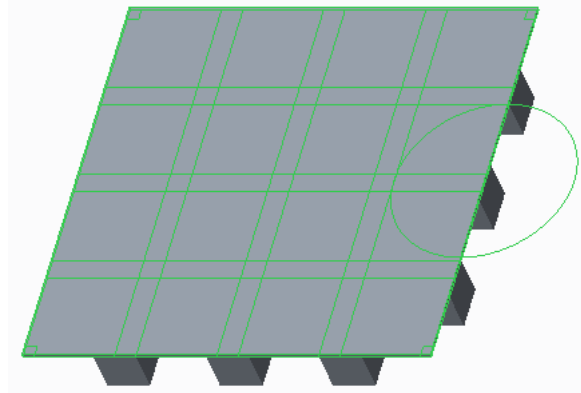


Figure 56: FEA model with grid mounting and load centered on the edge of the tile.

The results were collected for the von Mises stress distribution (Figure 57) and the maximum principal strain distribution (Figure 58).

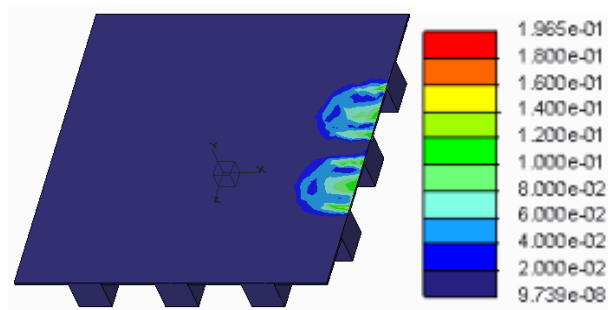


Figure 57: Von Mises stress distribution with grid mounting and load centered on the edge of the tile; units in MPa.

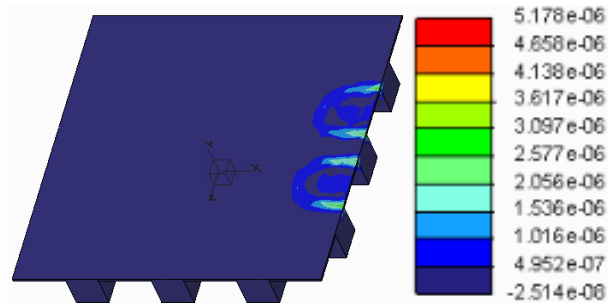


Figure 58: Maximum principal strain distribution with grid mounting and load centered on the edge of the tile; units in mm/mm.

A simulation was run when the load was applied on the corner of the tile, as shown in Figure 59.

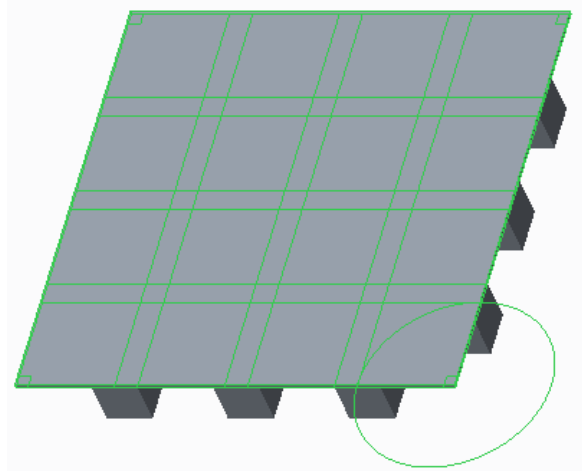


Figure 59: FEA model with grid mounting and load centered on the corner of the tile.

The results were collected for the von Mises stress distribution (Figure 60) and the maximum principal strain distribution (Figure 61).

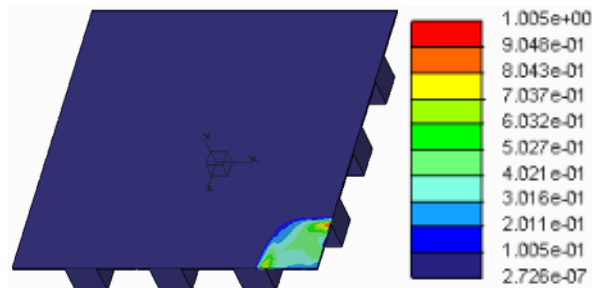


Figure 60: Von Mises stress distribution with grid mounting and load centered on the corner of the tile; units in MPa.

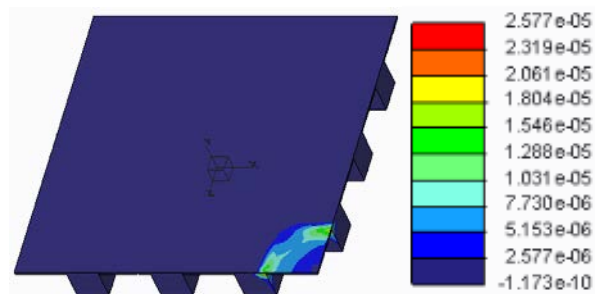


Figure 61: Maximum principal strain distribution with grid mounting and load centered on the corner of the tile; units in mm/mm.

Comparing these simulations demonstrates that the stress and strain are more localized when the ceramic is mounted on the laser-cut grid. When the film is mounted at the corners, there are strains at the corners in addition to a larger region where the load is applied. Also, the maximum strains for central loading scenarios are actually at a corner, so the location of the tap would be unclear. When the force is applied at a location in between the grid supports, the location of the tap can more easily and accurately be identified, as seen when comparing Figure 40 with Figure 52. When the

force is applied over the grid supports, the strain is spread across multiple squares on the tile, as seen in Figures 55 and 58. In future research, this phenomenon could be used in the location sensing algorithm to indicate a tap between two grid segments.

In addition, when the grid mounting was used, the maximum stress appeared to be much lower in all four scenarios, which is beneficial because it will reduce the likelihood of the ceramic breaking under pressure. The maximum strain values are also lower, but since it is more localized, this should not create a problem with location sensing.

### 4.2.3 Force vs. Voltage

Upon completion of the testing described in the methodology section of force vs. voltage, the results showed a linear relationship between the amount of force applied to the piezoelectric tile and the output voltage of the piezoelectric tile. The results of the testing including two calibration curves for two different days of testing and the changes in force and their voltages. One graph of a trial done with the 30 gram weight and Arduino at 130 speed can be seen in Figure 62. The maximum peak value at each point was recorded.

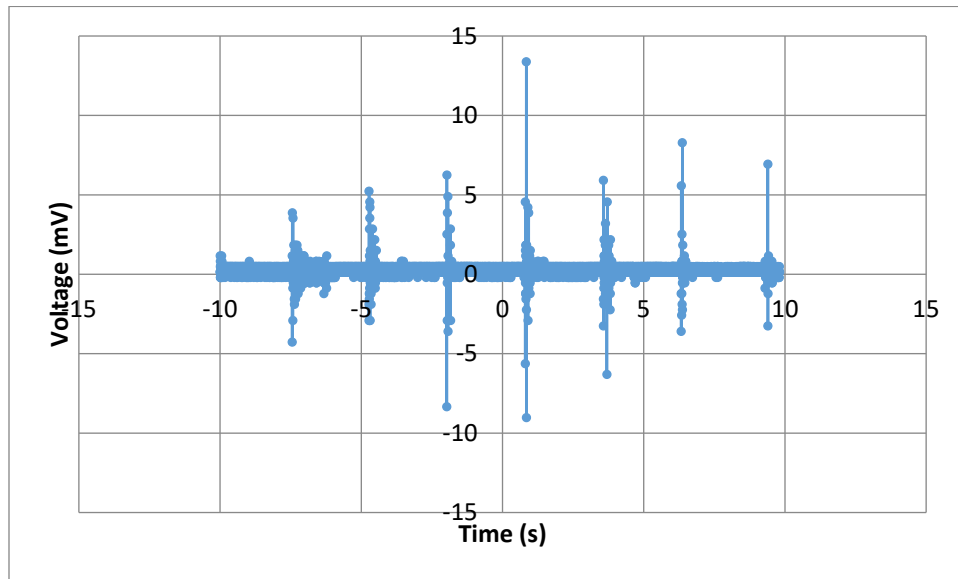


Figure 62: Voltage data from a trial using 30 grams and a stepper motor speed of 130.

The cumulative results are displayed in Figure 63 and Figure 64. Figure 63 displays the three median values for the peaks at each selected force. Figure 64 displays the 80% average value at each force. The data was graphed in such a way because there was an inconsistent number of data points at each force and extra points at a given force could skew the data set. From the surveys we discovered that the average force used was 0.0739 N which is the equivalent of 7.53 grams. This would make the max voltage we can expect in basic fully supported position around 1 or 2 mV.

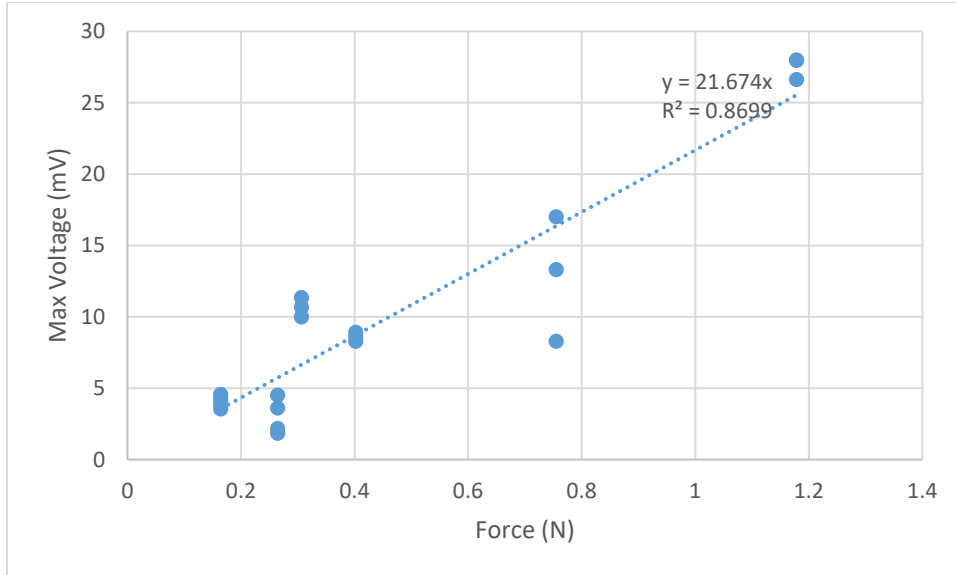


Figure 63: Data contains the three median values for the voltage peaks at each force.

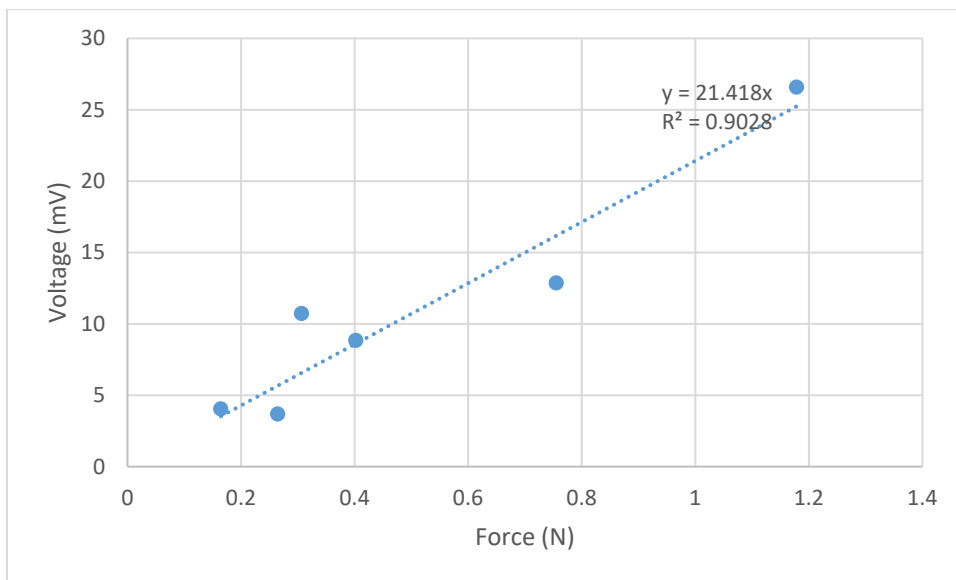


Figure 64: Data containing an 80% average value at each force.

To calculate the expected energy generated by one tap, the plot of voltage vs. time for one tap shown in Figure 65 was used. Then, the equation  $P = \frac{V^2}{R}$  was used to plot the power vs. time data shown in Figure 66. Finally, the area under this curve was found using the trapezoidal rule to give a value of  $6.6 \cdot 10^{-9}$  watt-hours per tap. Multiplying by the found 4,745 taps per day average found by the survey gives an estimated value of  $3.14 \cdot 10^{-5}$  watt hours per day generated by the piezoelectric element.

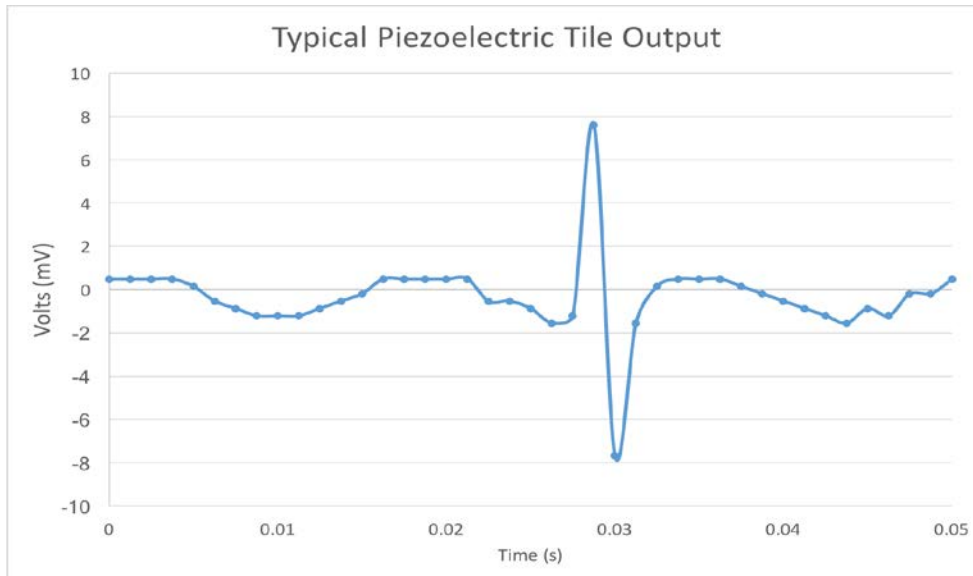


Figure 65: Plot of voltage vs. time for one tap using 30 g weight.

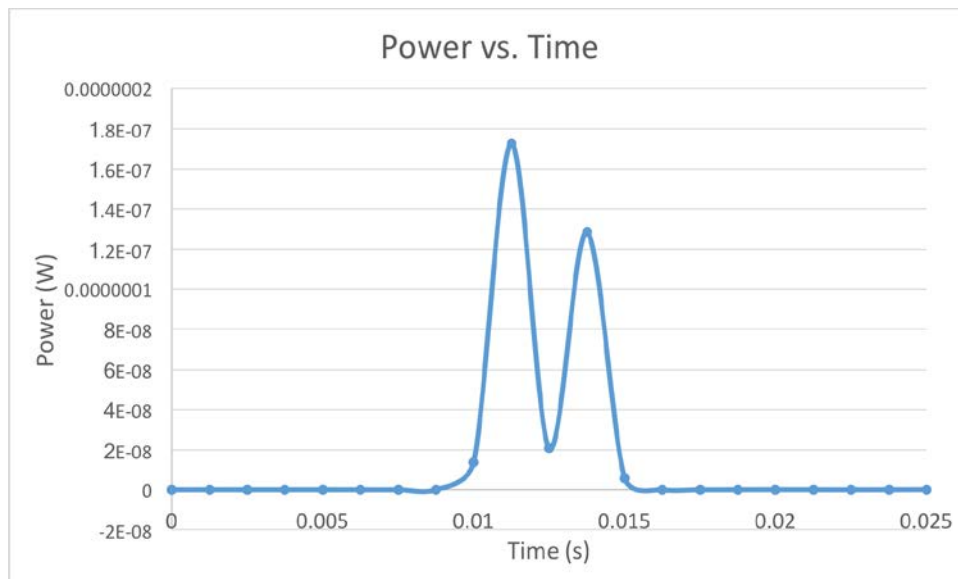


Figure 66: Plot of power vs. time for the same tap shown in Figure 64.

### 4.3 Circuits and Power Generation

While the results of the experimentation with the transformers and the bridge rectifier with standard diodes were important to the development of the project, the results themselves are not displayed. In both cases, all measurable output voltages consistently had no deviation from the standard offset values (usually less than 1 mV) that were present and measured by the oscilloscope; therefore, it can be assumed that their output was consistently zero.

When the bridge rectifier was remade with low voltage drop diodes, the results were non-zero. As shown in Figure 67, the rectified voltage from the piezoelectric device was actually able to impact the charge on the capacitor, though not to a significant degree.

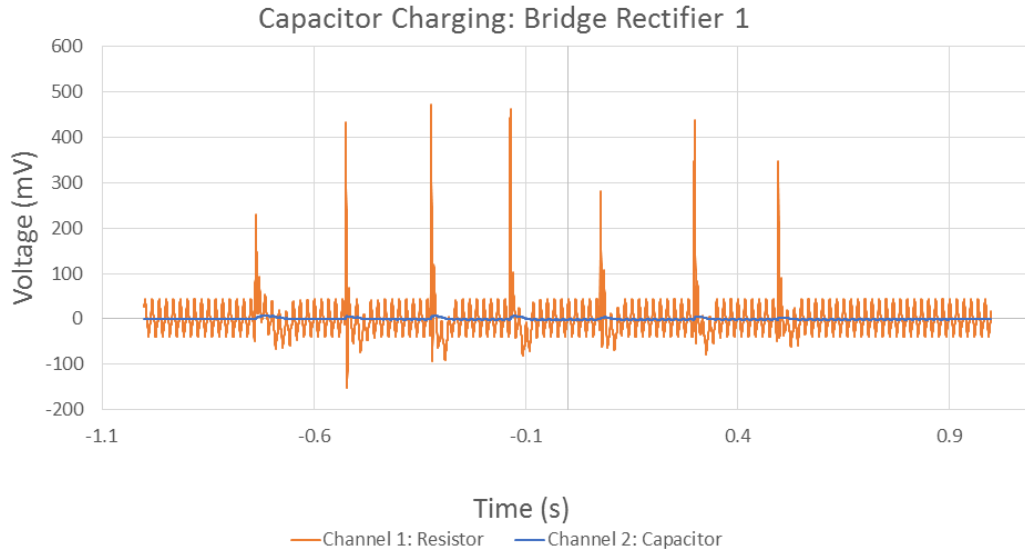


Figure 67: Voltage waveforms from testing with bridge rectifier and low voltage drop diodes.

Figure 68 displays the channel 2 capacitor data on a more visible scale. While the capacitors do temporarily get charged, it is at a very low voltage, and they clearly discharge before the next tap. On average, the capacitor's peak voltage was only 1.34% of the peak voltage across the resistor, which, as shown in previous testing is already quite low. The tapping rate for the testing was relatively quick, fitting seven individual taps in less than 1.5 seconds, but the duration of the capacitor's charge is not long enough for the next tap to further charge the capacitor. If the capacitor were ever to reach its maximum potential voltage difference, it would still need to still be holding charge when the next tap occurs.



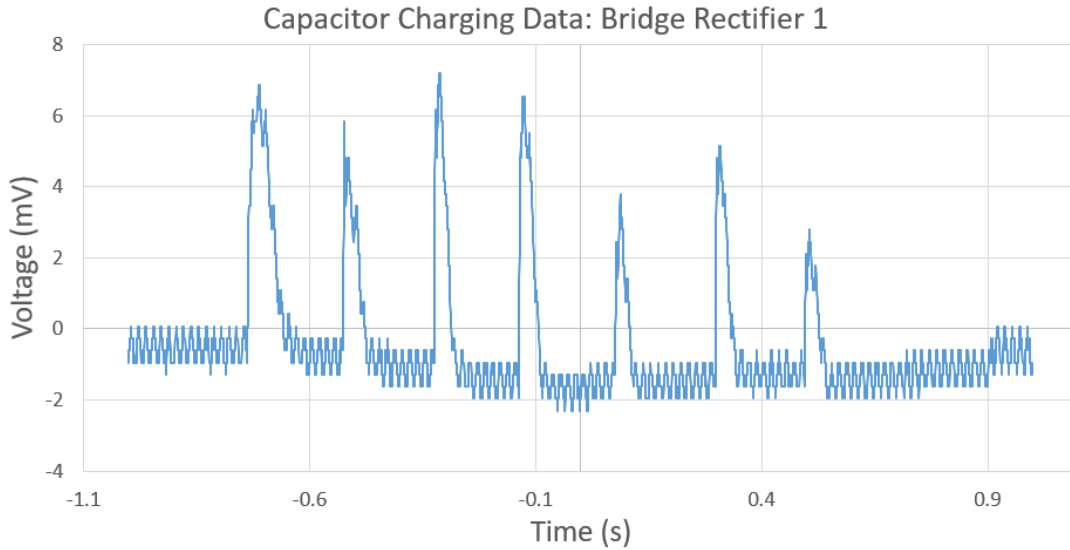


Figure 28: Magnified waveform of voltage across the capacitor from testing with bridge rectifier and low voltage drop diodes.

The half rectifier testing produced more variation in the waveforms measured across the resistor, but was generally able to produce more overall voltage than the full wave rectifier, both across the resistor and capacitor due to experiencing only a single diode voltage drop as opposed to two. The full data set from one testing period is shown in Figure 69 along with the capacitor data on a smaller scale.

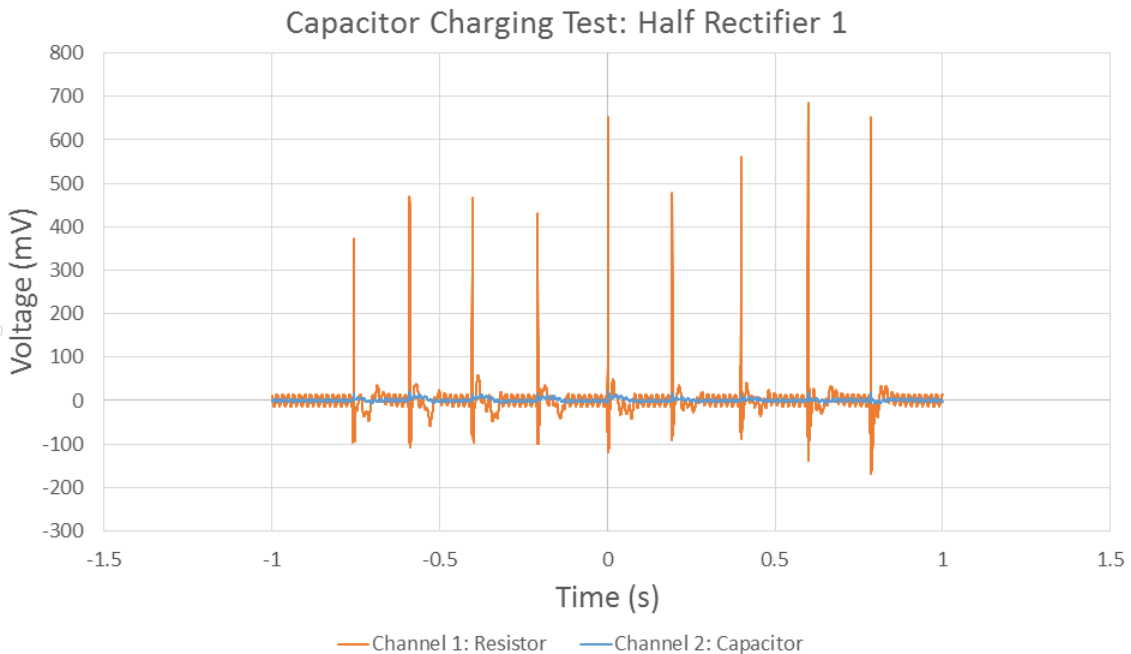
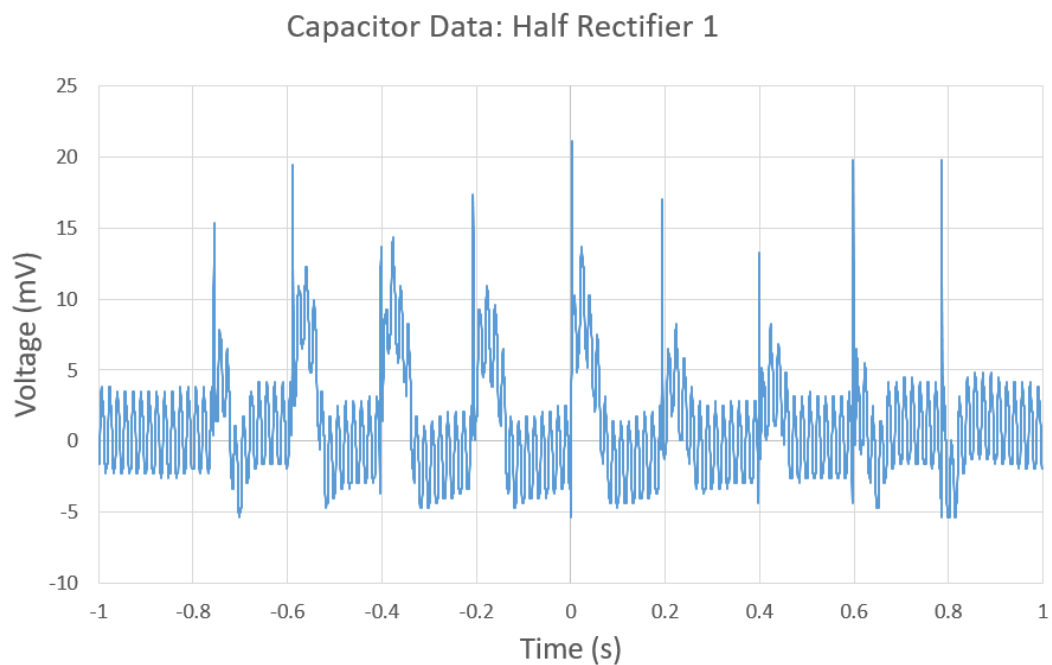


Figure 69: Voltage waveforms from testing with the half rectifier.



*Figure 70: Magnified waveform of voltage across the capacitor from testing with the half rectifier.*

The data was not highly consistent, but showed the potential for a higher overall peak voltage, averaging 4.57% of the peak voltage. Even this higher voltage is not enough to fully charge the 10 nF capacitor, so the half rectifier is not viable either, though it is potentially more promising should a higher piezoelectric output voltage be achieved in future research. That being said, the inconsistency of the results produced by this design, which occasionally produced a negative voltage across the capacitor, indicates that it is not a desirable choice for any charging circuit.

## 4.4 Prototyping

### 4.4.1 Voltage, Power, Waveform Characteristics

#### *Isolated Piezoelectric Tile*

The initial testing with an isolated piezoelectric tile in series with a 10k $\Omega$  resistor resulted in an AC waveform which quickly decayed in magnitude from its initial value. An example waveform is shown in Figure 71.

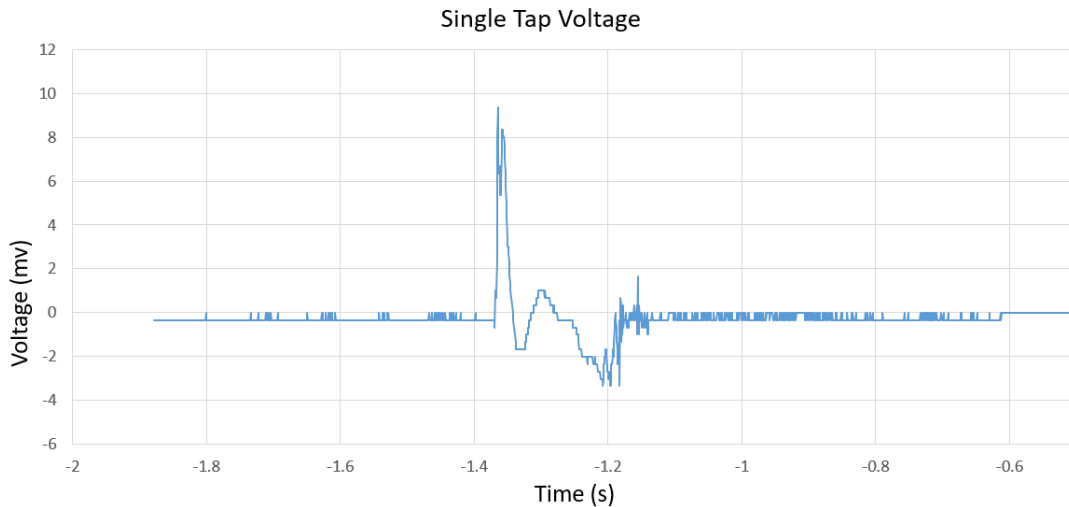


Figure 71: Voltage waveform from a single tap on an unaltered piezoelectric tile.

Typical test results showed an initial peak value averaging 10.5 mV. There was variation in the data due to the inconsistent force of the taps. The data was collected in three trials with three taps per trial. The waveforms consistently showed that higher maximum voltage correlated with a shorter rise time.

Table 7: Trial 1 data from unaltered piezoelectric tile.

	Tap 1	Tap 2	Tap 3	Average
Max mV	9.4	7.4	13.7	10.2
Rise Time	0.0031	0.0056	0.0025	

Table 8: Trial 2 data from unaltered piezoelectric tile.

	Tap 1	Tap 2	Tap 3	Average
Max mV	2.7	4.3	8.0	5.0
Rise Time	0.0137	0.0037	0.0012	

Table 9: Trial 3 data from unaltered piezoelectric tile.

	Tap 1	Tap 2	Tap 3	Average
Max mV	17.1	15.4	17.1	16.5
Rise Time	0.0019	0.0044	0.0019	

### ***Proof of Concept Etched Tile***

The proof of concept etched tile tests consistently showed differences between the output of the tapped and adjacent sections (Figure 72). Several comparisons were made: namely peak voltage values, and time delay between outputs.

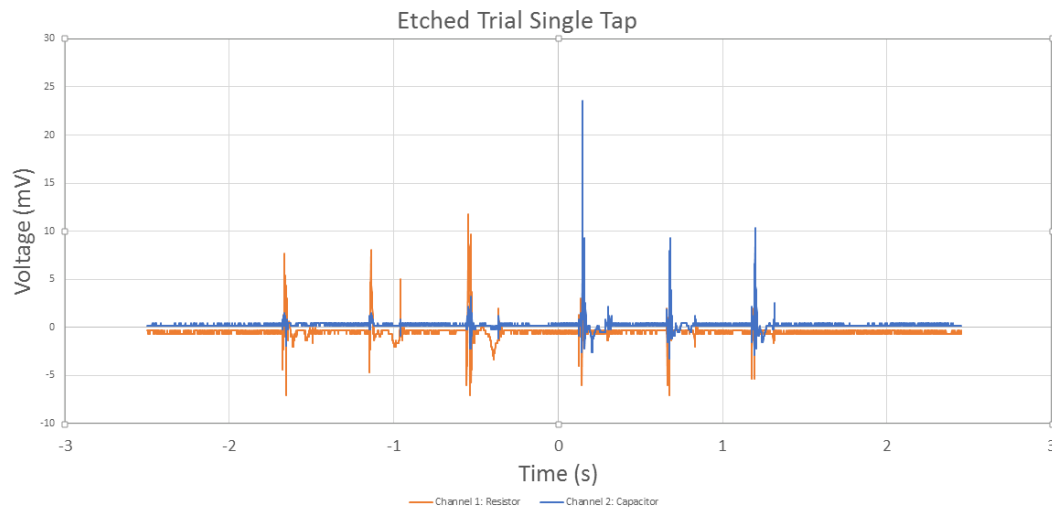


Figure 72: Voltage waveforms from proof of concept etched tile. The data consists of three taps on each section.

The trials were carried out with three taps on each side of the etched tile, with five total trials. The first tap of the first trial is shown on a smaller scale in Figure 73 so that it can be read more clearly.

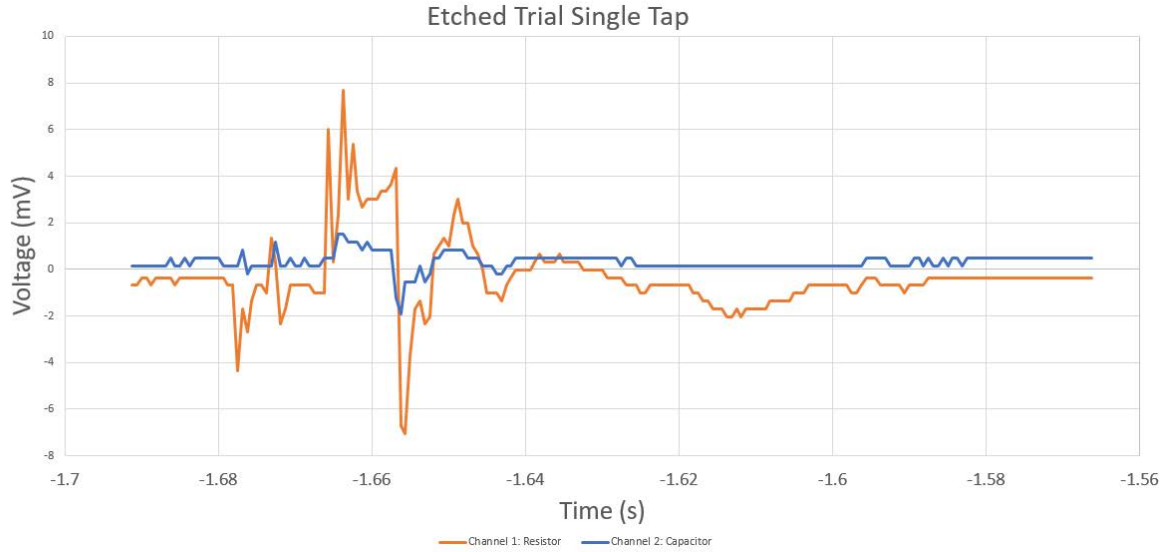


Figure 73: Magnified voltage waveform of the first tap from the proof of concept etched tile.

The results consistently showed the tapped side of the tile display a higher peak voltage than the untapped side. On average the untapped side peaked at 26.6% of the maximum value for the tapped side. Not only was this result consistent, but the difference is high enough that it can likely be used to detect location on a more complicated touchscreen prototype. The time difference was both small and inconsistent. The peak of the untapped side often occurred before the tapped side or at the exact same time; thus, it would be difficult and unrealistic to detect location based on this metric.

Table 10: Trial 1 data from proof of concept etched tile.

<b>Channel 1 Taps</b>	Tap 1	Tap 2	Tap 3	<b>Channel 2 Taps</b>	Tap 1	Tap 2	Tap 3
Ch1 max mV	7.7	8.0	11.7	Ch2 max mV	23.6	9.3	10.3
Ch2 max mV	1.2	1.2	1.8	Ch1 max mV	2.3	3.0	2.0
Ch1/Ch2	0.0869	0.0833	0.115	Ch2/Ch1	0.101	0.318	0.194
Time Diff	0.0013	0.0069	0.0056		0	-0.0019	-0.008125

Table 11: Trial 2 data from proof of concept etched tile.

<b>Channel 1 Taps</b>	Tap 1	Tap 2	Tap 3	<b>Channel 2 Taps</b>	Tap 1	Tap 2	Tap 3
Ch1 max mV	10.0	8.7	9.5	Ch2 max mV	6.2	7.0	5.2
Ch2 max mV	2.2	1.5	1.8	Ch1 max mV	1.0	1.7	0.3
Ch2/Ch1	0.134	0.0769	0.108	Ch1/Ch2	0.183	0.273	0.0732
Time Diff	0	0.5006	0		0.0006	0.0013	0.0031

Table 12: Trial 3 data from proof of concept etched tile.

<b>Channel 1 Taps</b>	Tap 1	Tap 2	Tap 3	<b>Channel 2 Taps</b>	Tap 1	Tap 2	Tap 3
Ch1 max mV	7.0	11.7	4.0	Ch2 max mV	3.9	5.2	8.3
Ch2 max mV	1.8	1.5	1.8	Ch1 max mV	2.0	2.7	2.3
Ch2/Ch1	0.143	0.0568	0.251	Ch1/Ch2	0.657	0.607	0.313
Time Diff	-0.0025	0.0038	0		-0.0056	-0.0656	-0.0006

Table 13: Trial 4 data from proof of concept etched tile.

<b>Channel 1 Taps</b>	Tap 1	Tap 2	Tap 3	<b>Channel 2 Taps</b>	Tap 1	Tap 2	Tap 3
Ch1 max mV	3.7	3.7	11.1	Ch2 max mV	3.5	0.4	2.5
Ch2 max mV	1.5	1.5	1.8	Ch1 max mV	1.0	0.1	0.7
Ch2/Ch1	0.272	0.272	0.121	Ch1/Ch2	0.327	0.357	0.326
Time Diff	0	-0.0019	0		0.0006	-0.0013	0.0013

Table 14: Trial 5 data from proof of concept etched tile.

<b>Channel 1 Taps</b>	Tap 1	Tap 2	Tap 3	<b>Channel 2 Taps</b>	Tap 1	Tap 2	Tap 3
Ch1 max mV	6.4	11.4	21.4	Ch2 max mV	4.9	2.9	2.9
Ch2 max mV	3.2	2.5	7.2	Ch1 max mV	2.3	0.2	0.7
Ch2/Ch1	0.372	0.148	0.300	Ch1/Ch2	0.575	0.822	0.325
Time Diff	-0.0038	-0.0006	-0.0038		0.0019	-0.0006	0

### **Prototype Etched Grid**

The testing for the 4x4 prototype etched grid showed less consistent results than the two-part tile due to the increased complexity of the system. The data shows comparisons between peak voltage values for several different grid segment combinations, including side to side, corner to corner, and adjacent corners of the grid.

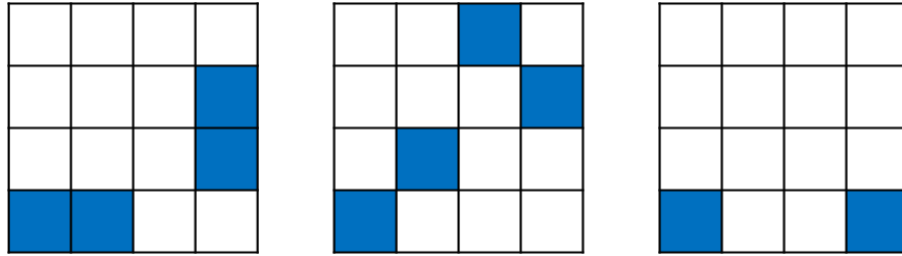


Figure 74: Examples of side to side, corner to corner, and adjacent corner grid sections.

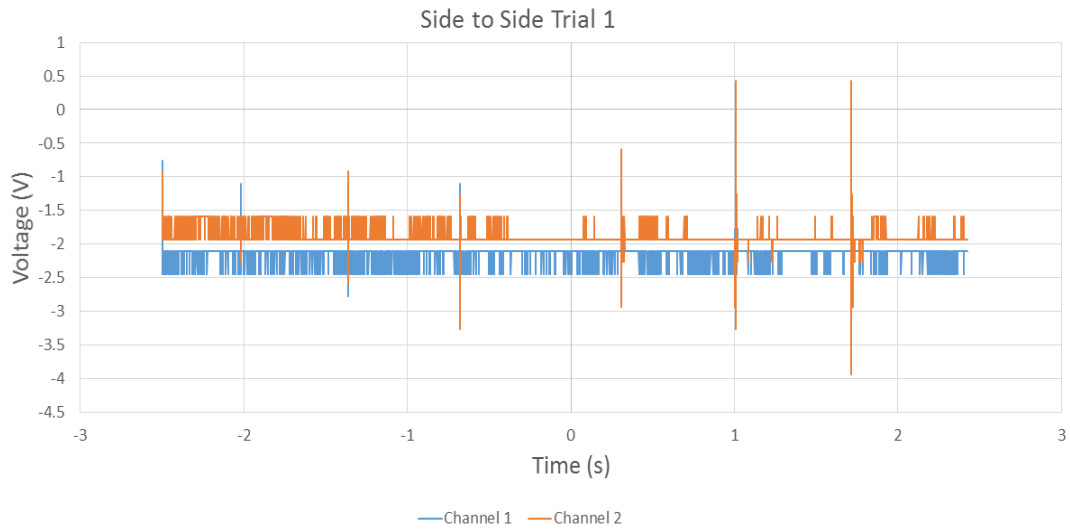


Figure 75: Voltage waveforms of two side by side prototype grid sections. The data consists of three taps on each section.

Table 15: Trial 1 data from side by side prototype grid sections.

<b>Channel 1 Taps</b>	Tap 1	Tap 2	Tap 3	<b>Channel 2 Taps</b>	Tap 1	Tap 2	Tap 3
Ch 1 max mV	-0.76	-1.1	-1.1	Ch 2 max mV	0.764	-0.25	-0.25
Ch 2 max mV	-1.93	-1.59	-1.93	Ch 1 max mV	-1.1	-1.43	-1.43
Ch 1 min mV	-2.44	-2.44	-2.11	Ch 2 min mV	-4.62	-2.26	-2.26
Ch 2 min mV	-3.94	-2.6	-2.6	Ch 1 min mV	-2.44	-2.11	-2.11
Ch2/Ch1	2.54	1.45	1.76	Ch1/Ch2	-1.44	5.85	5.85

Table 16: Trial 2 data from side by side prototype grid sections.

<b>Channel 1 Taps</b>	Tap 1	Tap 2	Tap 3	<b>Channel 2 Taps</b>	Tap 1	Tap 2	Tap 3
Ch 1 max mV	-0.8	-0.4	-0.4	Ch 2 max mV	0.4	-0.9	0.4
Ch 2 max mV	-1.3	-0.9	-0.9	Ch 1 max mV	-1.1	-1.1	-1.1
Ch 1 min mV	-2.1	-2.1	-2.1	Ch 2 min mV	-3.6	-1.9	-2.9
Ch 2 min mV	-2.3	-2.3	-2.6	Ch 1 min mV	-2.1	-2.1	-2.1
Ch2/Ch1	1.65	2.17	2.17	Ch1/Ch2	-2.56	1.19	-2.56

Table 17: Trial 3 data from side by side prototype grid sections.

<b>Channel 1 Taps</b>	Tap 1	Tap 2	Tap 3	<b>Channel 2 Taps</b>	Tap 1	Tap 2	Tap 3
Ch 1 max mV	-1.1	-1.1	-1.1	Ch 2 max mV	-1.77	-1.77	-1.43
Ch 2 max mV	-1.1	-0.92	-1.1	Ch 1 max mV	-0.58	0.427	0.427
Ch 1 min mV	-2.44	-2.78	-2.44	Ch 2 min mV	-2.44	-2.44	-2.78
Ch 2 min mV	-2.26	-2.6	-3.27	Ch 1 min mV	-2.93	-3.27	-3.94
Ch2/Ch1	1	0.837	1	Ch1/Ch2	0.328	-0.241	-0.298

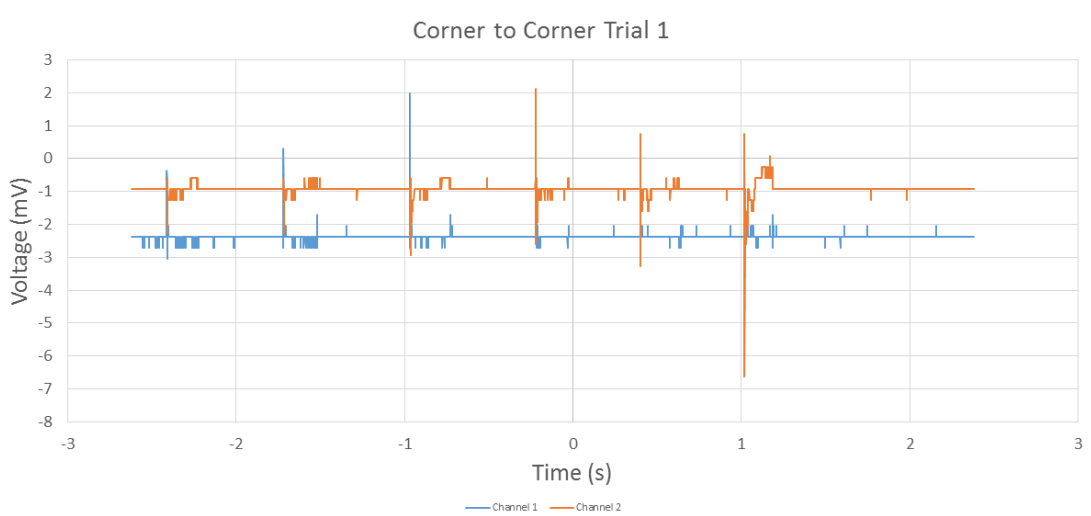


Figure 76: Voltage waveforms of two corner to corner prototype grid sections. The data consists of three taps on each section.



Table 18: Trial 1 data from corner to corner prototype grid sections.

<b>Channel 1 Taps</b>	Tap 1	Tap 2	Tap 3	<b>Channel 2 Taps</b>	Tap 1	Tap 2	Tap 3
Ch 1 max mV	-0.4	0.3	2.0	Ch 2 max mV	2.1	0.8	-0.9
Ch 2 max mV	-0.6	-0.6	-0.6	Ch 1 max mV	0.6	0.8	-2.4
Ch 1 min mV	-2.3	-2.7	-2.7	Ch 2 min mV	-2.6	-3.3	-0.9
Ch 2 min mV	-2.3	-2.3	-2.9	Ch 1 min mV	-2.4	-3.1	-0.9
Ch2/Ch1	1.58	-1.90	-0.292	Ch1/Ch2	0.305	1	2.60

Table 19: Trial 2 data from corner to corner prototype grid sections.

<b>Channel 1 Taps</b>	Tap 1	Tap 2	Tap 3	<b>Channel 2 Taps</b>	Tap 1	Tap 2	Tap 3
Ch 1 max mV	1.3	0	0.3	Ch 2 max mV	0.8	0.4	1.8
Ch 2 max mV	-0.9	-0.6	1.2	Ch 1 max mV	-0.4	-1.4	0
Ch 1 min mV	-2.4	-2.4	-2.4	Ch 2 min mV	-2.9	-2.6	-2.2
Ch 2 min mV	-2.4	-3.3	-3.9	Ch 1 min mV	-3.1	-2.6	-3.4
Ch2/Ch1	-0.684	18.7	4.03	Ch1/Ch2	-0.471	-3.10	-0.0169

Table 20: Trial 3 data from corner to corner prototype grid sections.

<b>Channel 1 Taps</b>	Tap 1	Tap 2	Tap 3	<b>Channel 2 Taps</b>	Tap 1	Tap 2	Tap 3
Ch 1 max mV	-0.4	1.3	2.3	Ch 2 max mV	0.1	1.1	3.1
Ch 2 max mV	-0.9	-0.9	-1.2	Ch 1 max mV	-1.0	-1.4	1.7
Ch 1 min mV	-2.4	-2.4	-2.4	Ch 2 min mV	-2.2	-3.3	-5.3
Ch 2 min mV	-2.4	-3.6	-4.3	Ch 1 min mV	-2.7	-2.7	-2.7
Ch2/Ch1	2.45	-0.684	-0.531	Ch1/Ch2	-9.66	-1.23	0.528

### Adjacent Corners Trial 1

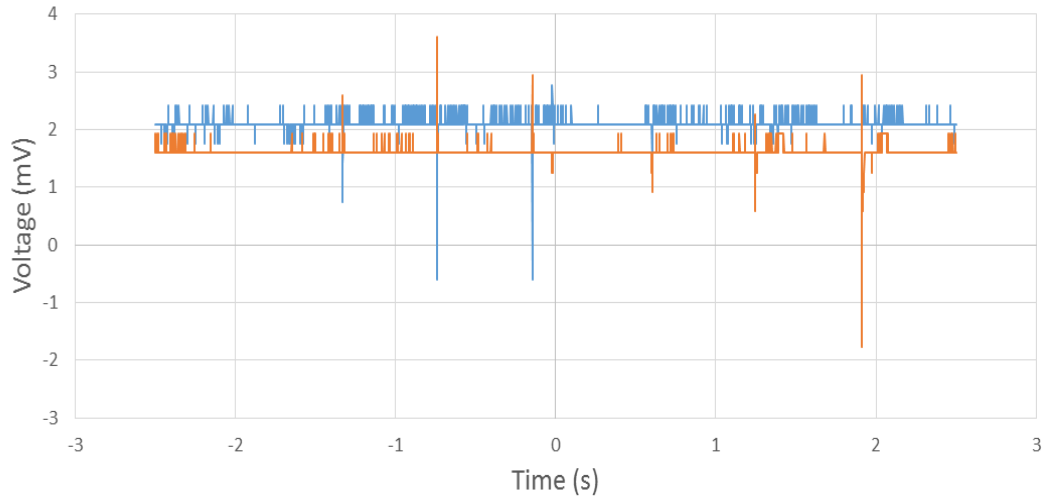


Figure 77: Voltage waveforms of two adjacent corner prototype grid sections. The data consists of three taps on each section.

Table 21: Trial 1 data from adjacent corner prototype grid sections.

<b>Channel 1 Taps</b>	Tap 1	Tap 2	Tap 3	<b>Channel 2 Taps</b>	Tap 1	Tap 2	Tap 3
Ch 1 max mV	-2.4	0.6	0.6	Ch 2 max mV	-0.9	-0.6	1.8
Ch 2 max mV	-1.6	-1.6	-1.6	Ch 1 max mV	-1.1	-1.8	-0.7
Ch 1 min mV	-2.4	-2.1	-2.9	Ch 2 min mV	-1.6	-2.3	-2.9
Ch 2 min mV	-2.6	-3.6	-2.9	Ch 1 min mV	-2.1	-2.3	-2.4
Ch2/Ch1	0.656	-2.62	-2.62	Ch1/Ch2	1.17	3.01	-0.418

Table 22: Trial 2 data from adjacent corner prototype grid sections.

<b>Channel 1 Taps</b>	Tap 1	Tap 2	Tap 3	<b>Channel 2 Taps</b>	Tap 1	Tap 2	Tap 3
Ch 1 max mV	0.9	0.9	-2.1	Ch 2 max mV	1.4	-0.9	0.4
Ch 2 max mV	-1.6	-1.3	-1.6	Ch 1 max mV	-0.4	-1.4	-1.4
Ch 1 min mV	-2.1	-2.1	-2.1	Ch 2 min mV	-2.6	-1.6	-2.3
Ch 2 min mV	-2.9	-3.9	-1.6	Ch 1 min mV	-2.1	-2.1	-2.1
Ch2/Ch1	-1.68	-1.33	0.761	Ch1/Ch2	-0.281	1.54	-3.31

Table 23: Trial 3 data from adjacent corner prototype grid sections.

<b>Channel 1 Taps</b>	Tap 1	Tap 2	Tap 3	<b>Channel 2 Taps</b>	Tap 1	Tap 2	Tap 3
Ch 1 max mV	-0.1	-0.7	-0.4	Ch 2 max mV	-0.6	-0.6	0.1
Ch 2 max mV	-1.6	-1.6	-1.6	Ch 1 max mV	-1.4	-1.1	-0.7
Ch 1 min mV	-2.4	-2.4	-2.1	Ch 2 min mV	-1.6	-1.6	-1.6
Ch 2 min mV	-2.6	-2.3	-2.3	Ch 1 min mV	-2.1	-2.4	-2.4
Ch2/Ch1	23.8	2.15	3.94	Ch1/Ch2	2.43	1.85	-8.13

The side to side trials were successful 13/18 times. The corner to corner trials were successful 16/18 times. The adjacent corner trials were successful 16/18 times. The “success” of these trials was defined as the tapped tile section resulting in a greater peak voltage (ratio of less than 1). The time difference was shown to be inconsistent in these trials as well, and it was determined to be a poor indicator of which section was tapped.

#### 4.4.2 Arduino Prototype

The Arduino code used maximum voltage as an identifier for the piezoelectric segment selection algorithm. Because the piezoelectric grid is not physically separated, all of the segments experience displacement and therefore generate a voltage regardless of where the impulse occurred. Based on the analysis of the waveforms, maximum voltage was determined to be one of the most effective identifiers, although it is not completely consistent. Different piezoelectric segments produce varying peak voltages based on their position in the grid. In order to account for these variations, multipliers were chosen for the analog values based on observational testing of the prototype grid. Further analysis of the waveforms or serial data could generate more accurate multipliers to improve the consistency of the response. Using the data from neighboring segments could also be used to improve consistency or to calculate location with greater precision.

The following data was collected from a prototype test using four segments of the 5x5 etched grid. The multipliers were modified between trials to attempt to improve the consistency of the test.

Table 24: Trial 1 data for prototype consistency testing.

<b>4 Tile Test</b>	Segment 1	Segment 2	Segment 3	Segment 4
Multiplier	1	6.4	2.3	0.9
success	18	14	20	17
no response	1	0	0	0
wrong output	1	6	0	3
trials	20	20	20	20

The second segment showed several failures where the output showed taps from the third or fourth segments instead. To address this, the segment 2 multiplier was raised from 6.4 to 7, the segment 3 multiplier was lowered to 2.1, the segment 4 multiplier was lowered to 0.7, and the segment 1 multiplier was raised to 1.2.

Table 25: Trial 2 data for prototype consistency testing.

<b>4 Tile Test</b>	Segment 1	Segment 2	Segment 3	Segment 4
Multiplier	1.2	7	2.1	0.7
success	15	18	19	15
no response	0	0	0	0
wrong output	5	2	1	5
trials	20	20	20	20

These changes showed improvements in segment 2, but the other segments performed worse. Segment 1 was raised further to 1.4, segment 4 was raised slightly to 0.75, and segment 3 was lowered further to 1.95.

Table 26: Trial 3 data for prototype consistency testing.

<b>4 Tile Test</b>	Segment 1	Segment 2	Segment 3	Segment 4
Multiplier	1.4	7	1.95	0.75
success	20	9	18	20
no response	0	1	0	0
wrong output	0	10	2	0
trials	20	20	20	20

The results for all segments except for segment 2 were consistently successful. Segment 2 performed worse than it had in previous tests, and further observation showed that it was often entirely unresponsive, which indicates that the problem was unrelated to the multipliers. Additional sources of error such as the quality of the soldered connections and inadequate support in the mounting system could have contributed to the failure rate and the large difference in the voltage output.

## Chapter 5: Conclusion

### *5.1 Summary of Results*

Team Piezo's goal for this project was to develop a prototype piezoelectric touchscreen with the ability to sense touch location, generate energy, and recharge a battery. Through FEA computer simulations, the team modeled the piezoelectric response to different loading conditions. This visualization of the stress and strain produced by various applied forces directed the team to mount the prototype on a laser cut grid matching the pattern of the etched electrodes. During testing, Team Piezo also showed a relationship between the voltage output and the force acting on the piezoelectric tile. The data from this test and the survey results were used to estimate the power/energy produced from a representative piezoelectric element at 113nJ per day.

The prototype successfully showed that location sensing could be accomplished by etching a grid pattern into the electrodes on both sides of a piezoelectric tile. This process creates electrically separated segments that experience varying voltage drops based on the location of the force applied to the piezoelectric tile. The etching process also allows the creation of leads to direct the energy generated from inner grid segments to the outer edge of the piezoelectric element for collection. Compared to the physically separated grid segment concept, the etched prototype has less wasted space between segments and allows multiple grid sections to generate useable energy from a single tap.

Although energy was generated by the piezoelectric element, the circuits that were tested to recharge a battery were unsuccessful. Forcing energy into a battery requires the voltage of the source to be higher than the voltage of the battery, which are typically at least nine volts. The voltage from the piezoelectric tile measured across a 10k $\Omega$  resistor was typically under 10mV from the prototype grid. The non-resonant waveform produced by tapping the piezoelectric element did not work with transformers, and charging a capacitor was unsuccessful because the negative voltages in the waveform caused immediate discharge.

### *5.2 Contributions*

Current research does not focus on the field of non-resonant piezoelectric systems. Team Piezo's development of a piezoelectric touchscreen prototype resulted in several important contributions to the field. Using a PZT ceramic material, the team conducted experiments to gather voltage waveform data produced by individual impulses on the piezoelectric element. Analysis of this data and further testing with several battery charging circuit concepts revealed several discrete characteristics of the waveform that prevented effective energy storage. Some of these characteristics include negative voltage peaks, low frequency, and fast decay. This information will be useful for future development of non-resonant piezoelectric systems.

Team Piezo also contributed to the field of piezoelectric sensing by proving that electrode etching could be used to electrically isolate grid sections and detect the

location of an applied force to a piezoelectric element. Other applications, such as feedback systems for robotics, could also benefit from this technology.

Lastly, there are also several advantages a piezoelectric touchscreen would have over current resistive and capacitive touchscreen technologies. One major aspect for resistive touchscreens is multi-touch capabilities. These touchscreens are unable to process more than one touch at a time due to their single sheet design, while piezoelectric touchscreens would be able to support this function with their multi-section design. In capacitive touchscreens, one of the limiting factors is that a finger or specially designed conductive material must be used with the screen. However, because piezoelectric touchscreens are based on physical and not electrical impulses, any material could be used. Lastly, some current iPhones have a function called Force Touch in which soft and heavy taps can be distinguished for different functions. A piezoelectric material would be able to sense a gradient of forces and could provide more versatility for touch applications. Overall, there are several improvements a piezoelectric touchscreen could provide over resistive and capacitive touchscreens.

### ***5.3 Recommendations for Future Work***

The piezoelectric grid touchscreen prototype could benefit from future work to make it a marketable product. Continuing to miniaturize the grid and improve the location selection algorithm would be necessary to compete with the precision of capacitive touchscreens that are currently in use. Improving the theoretical model of the piezoelectric touchscreen to gain a thorough understanding of the element's reaction to a tap would be useful for the algorithm development. The etched piezoelectric grid would also have to be tested in an assembled touchscreen with the LCD and protective layers.

Similarly, the assembled prototype would have to be tested for durability, since smartphones are often dropped. It is likely that a different piezoelectric material would be better suited for use in a smartphone because the ceramic used in the prototype is brittle. A material that is more durable and flexible would be optimal for the design. In addition, the hand-soldered connections used in the prototype were bulky and inconsistent. The final product would need an improved method of connecting to the electrode segments and analyzing the signals from the touch screen.

In addition to improving the location sensing aspect of the touchscreen, more research is required to develop an effective energy harvesting circuit for charging a battery. Reducing the thickness of the piezoelectric tile would cause more stress, which would generate higher voltages. Thinner piezoelectric elements would also allow several layers to be used in a single screen, which would significantly increase the amount of power that could be collected. Modifying the mounting system so it doesn't dampen, but possibly even amplifies, the resonant properties of a piezoelectric device could improve the charging behavior. More complex circuit designs that have a similar effect or store small amounts of energy efficiently could be designed and tested to allow energy storage. These and other improvements may depend on technological

advancements in other fields such as piezoelectric materials with greater inherent power generation capabilities or diodes with lower voltage drops.

Based on the low value of energy produced from the current piezoelectric system, future work would need to increase the piezoelectric element's performance to make a significant difference compared to the amount of energy consumed by a smartphone. Because the most important benefit of a piezoelectric touchscreen over current technology would be its ability to generate useable energy, both the energy generation and storage would have to be improved. As the piezoelectric technology improves, piezoelectric touchscreens will become a viable option for touchscreen devices.

## Glossary

**Alternating current (AC):** current in which the flow of electrons alternates direction

**Bi-stable system:** a structure that has two stable mechanical shapes

**Cantilever Mount:** a beam with all six degrees of freedom fixed at one edge

**Charge:** the quantity describing the force experienced by an object in an electromagnetic field. In a circuit, charge is related only to the number of electrons

**Coulombs:** the SI unit measurement of the amount of charge transferred in one second across a conductor in a constant current of one ampere

**Current:** the time rate of flow of electric charge, in the direction that a positive moving charge would take and having magnitude equal to the quantity of charge per unit time: measured in amperes

**D<sub>33</sub>:** the piezoelectric charge coefficient which describes how much current can be generated from a piezoelectric material when a perpendicular force is applied; has units of picocoulombs ( $10^{-12}$  coulombs) per Newton

**Denton E-beam Evaporator:** instrument that bombards the (ITO) anode with an electron beam, making (ITO) atoms go into the gaseous phase and then precipitate onto the sample

**Diode:** electrical component of a semiconductor, with a positive electrode on one end (cathode) and a negative electrode on the other (anode); has little to no resistance in one direction and higher resistance in the opposite direction as current passes through

**Direct current (DC):** current in which the flow of electrons travels in one direction

**Electric Dipole:** the separation of two charges (positive and negative), generally equal in magnitude and placed near each other.



**Ferroelectrics:** a property of certain materials that contain a spontaneous electric polarization that can be reversed by applying an external electric field

**Grid:** the system in which electrical power is generated and consumed

**Indium Tin Oxide (ITO):** a transparent conducting oxide, includes properties of electrical conductivity and optical transparency

**KNN-LT-LS:** potassium sodium niobate-LiTaO<sub>3</sub>-LiSbO<sub>3</sub> Piezoelectric ceramic system

**Light emitting diode (LED):** a diode that has a small light to indicate that current is flowing through it

**Mechanical strain:** deformation of a material as a result of an applied force

**Non-Resonant:** the lack of or inability of a system to increase in amplitude of oscillation when a force is applied at the same frequency

**Parallel:** components in a circuit are connected parallel to one another, and all components receive the same voltage

**Piezoelectric materials:** certain materials that can produce electricity when pressure is applied

**PZN-9PT:** Pb(Zn<sub>1/3</sub>Nb<sub>2/3</sub>)O<sub>3</sub>-9%PbTiO<sub>3</sub> piezoelectric ceramic

**PZT:** lead zirconate titanate. One of the most widely used piezoelectric ceramic materials

**Rectilinear:** contained by, consisting of, or moving in a straight line or lines.

**Resistance:** the opposition to the passage of an electric current through a conductor; a measure of how much an electrical conductor opposes the flow of electrons

**Root Mean Square:** In mathematics, the root mean square (abbreviated RMS or rms), also known as the quadratic mean, is a statistical measure of the magnitude of a varying quantity.

**Series:** components in a circuit are connected along a single path, allowing the same current to travel to all components

**State of Charge:** the equivalent of a fuel gauge for the battery. The units of SOC are percentage points (0% = empty; 100% = full).

**Uniaxial:** having only one axis

**Voltage:** the potential energy change of a unit charge moving from one location to another

**Wood's Metal:** a low-temperature solder; an alloy of bismuth, lead, tin, and cadmium

## Bibliography

Abazari, M., Choi, T., Cheong, S., & Safari, A. (2010). Nanoscale characterization and local Piezoelectric properties of lead-free KNN-LT-LS thin films. *Journal of Physics D: Applied Physics*, 43(2), 025405. doi:10.1088/0022-3727/43/2/025405

Apple. (2017). Apple Product Information Sheet 4.18.17. Retrieved May 2, 2017, from <https://www.apple.com/legal/more-resources/docs/apple-product-information-sheet.pdf>.

Benham, P., & Crawford, R. (n.d.). *Mechanics of engineering materials*.

Betts, D. N., Kim, H. A., Bowen, C. R., & Inman, D. J. (2012). Optimal configurations of bistable Piezo-composites for energy harvesting. *Applied Physics Letters*, 100(11), 114104. doi:10.1063/1.3693523

Carroll, A., & Heiser, G. (2010). An Analysis of Power Consumption in a Smartphone. 2010 USENIX Annual Technical Conference. Retrieved May 2, 2017, from [https://www.usenix.org/legacy/event/usenix10/tech/full\\_papers/Carroll.pdf](https://www.usenix.org/legacy/event/usenix10/tech/full_papers/Carroll.pdf).

Charging lithium ion batteries. (2003). Retrieved from [http://batteryuniversity.com/learn/article/charging\\_lithium\\_ion\\_batteries](http://batteryuniversity.com/learn/article/charging_lithium_ion_batteries)

Choy, S. (2007). Study of BNT-BKT-BT lead-free Piezoelectric ceramics and their application in Piezoelectric devices (Thesis). The Hong Kong Polytechnic University.

Retrieved from <http://repository.lib.polyu.edu.hk/jspui/handle/10397/3383>

Dayou, J., Man-Sang, C., Dalimin, M. N., & Wang, S. (2009). Generating energy using Piezoelectric material. *Borneo Science*. 24.1: 48-51. Retrieved from

<http://wwwsst.ums.edu.my/data/file/SqD1WjfN7sf2.pdf>

eMarketer. (2014). 2 Billion Consumers Worldwide to Get Smart(phones) by 2016.

Retrieved December 15, 2015, from <http://www.emarketer.com/Article/2-Billion-Consumers-Worldwide-Smartphones-by-2016/1011694>.

EPA. (2014). eGRID (Rep.). Retrieved April 2, 2017, from <http://www.epa.gov/egrid>

Gilbert, J. A., Ph.D., & Carmen, C. L., Ph.D. (2011, July). MAE/CE 370 -

MECHANICS OF MATERIALS - LABORATORY MANUAL. Retrieved from

<http://concretecanoe.org/Webmaster/Resume/CourseNotes/NOTES4.pdf>

Goldfarb, M., & Jones, L. (1999). On the efficiency of electric power generation with Piezoelectric ceramic. *Journal of Dynamic Systems, Measurement, and Control*, 121(3), 566-571. doi:10.1115/1.2802517.

Helman, C. (2013). How Much Electricity Do Your Gadgets Really Use? *Forbes*.

Retrieved April 02, 2017, from

<https://www.forbes.com/sites/christopherhelman/2013/09/07/how-much-energy-does-your-iphone-and-other-devices-use-and-what-to-do-about-it/#45e2f9232f70>

Henderson, T. (2009). Energy harvesting dance floors. *Energy Harvesting Journal*. Retrieved from <http://www.energyharvestingjournal.com/articles/energy-harvesting-dance-floors-00001613.asp?sessionid=1>

How does a touchscreen phone work? (2011). Technessitivity. Retrieved from <http://www.technessitivity.com/2011/07/how-do-touch-screens-work-infographic/>

Huq T. R., & Williamson, S. S. (2013). Comprehensive comparative analysis of Piezoelectric energy harvesting circuits for battery charging applications. *IEEE Xplore*, 6698 - 6702. doi:10.1109/IECON.2013.6700241

Kim, S., Clark, W. W., & Wang, Q. M. (2005). Piezoelectric energy harvesting with a clamped circular plate: experimental study. *Journal of Intelligent Material Systems and Structures*, 16(10), 855-863.

Neamtu, O., & Kokkosis, A., (2012). A Piezoelectric energy harvesting converter for charging lithium-ion battery. *Journal of Electrical & Electronics Engineering*, 5(1), 141-144. Retrieved from <http://search.ebscohost.com/login.aspx?direct=true&db=aph&AN=79369486&login.aspx&site=ehost-live>

Pavlic, J., Malic, B., & Rojac, T. (2014). Small reduction of Piezoelectric d33 response in Potassium Sodium Niobate Thick Films. *Journal of the American Ceramic Society*, 97(5), 1497-1403. doi:10.1111/jace.12797.

Phone Addict. (2013). Retrieved from <http://sunnyspeed.com/addict/>.

PhoneArena Team (2008). Article: touchscreen technologies in phones. Retrieved from [http://www.phonearena.com/news/Article-Touchscreen-technologies-in-phones\\_id3067](http://www.phonearena.com/news/Article-Touchscreen-technologies-in-phones_id3067)

Piezotech S.A.S. (n.d.). Piezoelectric films technical information. Retrieved from <http://www.Piezotech.fr/image/documents/22-31-32-33-Piezotech-Piezoelectric-films-leaflet.pdf>

Prasannablalaji, V., Rakesh, R., Sairam, S., & Mahesh, S. (2013). Staircase power generation using Piezo-electric transducers. *Advance in Electronic and Electric Engineering*, 3(6), 747-754. Retrieved from [http://www.ripublication.com/aeee/014\\_pp%20%20%20%20%20747-754.pdf](http://www.ripublication.com/aeee/014_pp%20%20%20%20%20747-754.pdf)

Saini, S. (2011). How do touch-sensitive screens work? Retrieved from <http://engineering.mit.edu/ask/how-do-touch-sensitive-screens-work>

Sirohi, J. & Inderjit, C. (2000). Fundamental understanding of Piezoelectric strain sensors. *Journal of Intelligent Material Systems and Structures*, 11(4), 246-257. doi: 10.1106/8BFB-GC8P-XQ47-YCQ0

Sodano, H., Inman, D., & Park, G. (2004). A Review of Power Harvesting from Vibration using Piezoelectric materials. *Shock and Vibration Digest*, 36(3),197-206. Retrieved from <http://mesl.ucsd.edu/gupta/SHM/EHW/SVD%202004-power%20harvesting1.pdf>

Telba, A., & Ali, W. (2012). Modeling and simulation of Piezoelectric energy harvesting. In *Proceedings of the World Congress on Engineering 2012*, 2. Retrieved from [http://www.iaeng.org/publication/WCE2012/WCE2012\\_pp959-961.pdf](http://www.iaeng.org/publication/WCE2012/WCE2012_pp959-961.pdf).

Teiche, A., Rai, A. K., Yane, C., Moore, C., Solms, D., Çetin, G., Riggio, J., Ramseyer, N., D'Intino P., Muller, L., Khoshabeh, R., Bedi, R., Bintahir, M. T., Hansen, T., Roth, T., & Sandler, S. (2009). Multitouch Technologies. Retrieved from [https://bramvandeputte.files.wordpress.com/2011/04/multi-touch\\_technologies\\_v1-01.pdf](https://bramvandeputte.files.wordpress.com/2011/04/multi-touch_technologies_v1-01.pdf)

Touching the future. (2008). *The Economist*. Retrieved from <http://www.economist.com/node/11999181>

Ryall, J. (2008). Japan harnesses energy from footsteps. *The Telegraph*. Retrieved from <http://www.telegraph.co.uk/earth/energy/3721841/Japan-harnesses-energy-fromfootsteps.html>

Wikipedia. (2017). Deformation (engineering). Retrieved March 26, 2017, from [https://en.wikipedia.org/wiki/Deformation\\_\(engineering\)#/media/File:Stress-strain1.svg](https://en.wikipedia.org/wiki/Deformation_(engineering)#/media/File:Stress-strain1.svg)

Wilson, T. V., Chandler, N., Fenlon, W., & Johnson, B. (2007). How the iPhone works. *How stuff works*. Retrieved from <http://electronics.howstuffworks.com/iphone1.html>.

Woodford, C. (2014). Piezoelectricity. *Explain that stuff*. Retrieved from <http://www.explainthatstuff.com/Piezoelectricity.html>

Zhao, P., Zhang, B.-P., & Li, J.-F. (2007). High Piezoelectric  $d_{33}$  coefficient in Li-modified lead-free (Na,K)NbO<sub>3</sub> ceramics sintered at optimal temperature. *Applied Physics Letters*, 90, 242909. doi:10.1063/1.2748088